THE JOURNAL OF COMPARATIVE NEUROLOGY 372:597–617 (1996)

Distribution and Coverage of Beta Cells in the Cat Retina

J.J. STEIN, S.A. JOHNSON, AND D.M. BERSON
Department of Neuroscience, Division of Biology and Medicine, Brown University, Providence, Rhode Island 02912

ABSTRACT

We have reexamined the retinal distribution and dendritic field dimensions of beta cells in the cat retina. Beta cells were labeled by retrograde transport from the A-layers of the lateral geniculate nucleus and distinguished from alpha cells on the basis of soma size. Dendritic fields of beta cells were visualized by intracellular staining in vitro. The fraction of cat ganglion cells that were beta cells varied with retinal location. Except near the area centralis, beta cells represented about half of all ganglion cells in the nasal hemiretina. They contributed as heavily as the other major ganglion cell classes to the nasal visual streak. In and near the area centralis and in the temporal retina, beta cells represented about two-thirds of all ganglion cells.

The areas of beta cell dendritic fields were reciprocally related to beta cell density. For example, they were 3-fold smaller within the visual streak than at matched eccentricities outside it. For many cells, we could estimate both local beta cell density and dendritic field area. Coverage factor (dendritic field area × local density) remained constant at about 4 despite 100-fold variations in beta cell density, and was independent of eccentricity, nasotemporal location, or position relative to the visual streak. Analysis in terms of sampling theory suggests that the beta cell array is matched to X-cell spatial resolution so as to optimize acuity. The beta cell distribution and its systematic reflection in dendritic architecture predict acuity levels that apparently correlate well with actual visual performance across the cat's visual field.

Indexing terms: X-cells, lateral geniculate nucleus, ganglion cells, acuity

Beta cells are a well-established morphological class of cat retinal ganglion cells that corresponds to the physiologically defined X-cell class (for reviews see Lennie, 1980; Sherman and Spear, 1982; Stone, 1983; Sherman, 1985). These ganglion cells have been implicated in high-resolution pattern vision by their high spatial density, small dendritic fields and receptive fields, and prominent contribution to cortical visual mechanisms (e.g., Sherman and Spear, 1982; Stone, 1983; Sherman, 1985; Pasternak and Horn, 1991; Wässle and Boycott, 1991).

It is of interest to know how beta cells are distributed and how their dendritic field dimensions vary across the retina because these factors may constrain the resolving power of the X-cell system (Peichl and Wässle, 1979; Hughes, 1981a; Wässle and Boycott, 1991). It is generally accepted that the ratios of beta (or X) cells to alpha (or Y) cells is higher in the central retina than in the periphery (e.g., Cleland et al., 1973; Fukuda and Stone, 1974; Wässle et al., 1975; Leventhal, 1982; Stone, 1983), but otherwise there has been considerable controversy about the beta cell distribution. According to one view (Illing and Wässle, 1981; Wässle et al., 1981a), beta cells represent a constant fraction of ganglion cells everywhere. This implies that the form of the beta cell distribution resembles that for all ganglion cells, including its visual streak, a horizontal ridge of elevated cell density (e.g., Stone, 1978; Hughes, 1981b; Wong and Hughes, 1987). An alternative view (Rowe and Stone, 1976; Stone and Keens, 1980; Rowe, 1990) is that the beta cell distribution is radially symmetrical about the area centralis, whereas the visual streak results primarily from the concentration of ganglion cells that are neither beta nor alpha (often collectively termed "gamma" cells). A third perspective is that the relative frequency of beta cells is higher in the central than in the peripheral retina (Peichl and Wässle, 1979; Hughes, 1981b).

The discrepancies among these studies are partly attributable to the use of soma size to distinguish beta cells from gamma cells, an approach complicated by the substantial overlap between the soma size spectra of these cell classes (Leventhal et al., 1980, 1985; Stone and Clarke, 1980; Rowe and Dreher, 1982; Dacey, 1989; Pu et al., 1994), and by a

Accepted April 11, 1996.

Address reprint requests to Dr. David Berson, Department of Neuroscience, Box 1953, Brown University, Providence, RI 02912. E-mail: David_Berson@brown.edu

lack of consensus about how beta cell soma size varies across the retina (Rowe and Stone, 1976; Stone and Keens, 1980; Hughes, 1981b).

In this study, we have exploited the output specificities of beta cells to distinguish them from other ganglion cells and to determine their retinal distribution. All beta and alpha cells project to the A-laminae of the lateral geniculate nucleus (LGN) while no other neurons of the ganglion cell layer do so (Kelly and Gilbert, 1975; Illing and Wässle, 1981; Itoh et al., 1981; Leventhal, 1982; Stone, 1983; Leventhal et al., 1985; Sherman, 1985; Hsiao and Sherman, 1986; but see Cleland et al., 1976). We were thus able to use retrograde tracers to mark beta and alpha cells selectively; beta cells were then easily distinguished from alpha cells at any eccentricity on the basis of soma size (Boycott and Wässle, 1974; Wässle et al., 1975; Kolb et al., 1981; Leventhal, 1982; Leventhal et al., 1985). We stained some of the labeled cells by intracellular dye injection in vitro to confirm their identity as beta cells. This also provided independent evidence on the beta cell distribution, because the dendritic field sizes of beta cells are presumably inversely proportional to local beta cell density (Fischer, 1973; Wässle et al., 1981b; Dacey, 1989, 1993; Wässle and Boycott, 1991).

MATERIALS AND METHODS

Retrograde labeling of beta cells

Retinal ganglion cells projecting to the A-layers of the lateral geniculate nucleus were labeled by retrograde transport in 12 adult cats. We used two different retrograde tracers with complementary attributes. To saturate large parts of the geniculate topography (at the risk of some involvement of surrounding structures), we used horseradish peroxidase (HRP), a tracer that diffuses readily. To make smaller deposits that could be unambiguously restricted to the A-layers, we used rhodamine-labeled latex microspheres ("beads"), a marker with negligible diffusion. Techniques for tracer injection, tissue processing and plotting of cell distributions have been described in detail elsewhere (Berson and Stein, 1995; Stein and Berson, 1995). All surgery was done under aseptic conditions in animals deeply anesthetized with Nembutal (35 mg/kg i.p., supplemented as needed i.v.).

In 5 cats, the retrograde tracer was horseradish peroxidase (HRP; Type VI; Sigma, St. Louis, MO; 10–15% w/v in 0.1 M Tris buffer, pH 7.4 or 0.05 M NaCl) while in 7 others, the tracer consisted of undiluted fluorescent beads (Lumafluor, New City, NY or Molecular Probes, Eugene, OR). In four of the bead experiments (cats G6, G8, G9, and G13) the geniculate injections were bilateral. Because the laminar LGNs on the two sides receive input from nonoverlapping retinal regions, we were able to analyze independently the retinal labeling patterns evoked from each LGN. The two sets of data in such cases will be distinguished below by appending "L" or "R" (for left or right LGN deposit, respectively) to the identifier for the animal (e.g., "G13L"). Tracers were injected pneumatically through a micropipette (tip diameter 20–50 μm). Deposit sites were targeted by stereotaxis, extracellular multiunit recordings made through the injection pipette, and reference to the map of Sanderson (1971). When our goal was to saturate as large a fraction of the geniculate A-layers as possible, we made as many as 64 separate deposits of HRP, delivering total volumes up to 2 μl. In other experiments, we reduced or eliminated involvement of structures outside the A-layers by limiting the number and volume of HRP deposits, or by using the beads.

Approximately 48 hours after HRP injections or 2–7 days after bead injections, animals were given an overdose of Nembutal and the eyes were removed and processed as described below. The brain was fixed by intravascular perfusion and cut on a freezing microtome as previously described (Berson and Stein, 1995). Sections through bead deposits were mounted without dehydration or clearing and examined by epifluorescence microscopy. To visualize HRP deposits, we reacted selected sections with a conventional histochemical method (Hanker et al., 1977). Incubation periods were truncated as necessary to preserve differences in staining density between the core and periphery of the deposit and to keep the tissue from becoming too brittle.

Living retinas were isolated just after eye removal, mounted on filter paper (Pu and Berson, 1992) and, except in intracellular staining studies, fixed immediately by immersion in buffered 4% paraformaldehyde for 20 minutes (HRP experiments) or several hours (bead experiments). For HRP studies, retinas were processed as by Leventhal et al. (1985) except that 1% dimethyl sulfoxide was included in all steps. Retinas were mounted using a protocol that induces no detectable shrinkage of the retina in the plane of the wholemount (Berson and Stein, 1995).

Mapping the distributions of labeled ganglion cells

Retinal wholemounts were analyzed at total magnifications of 50–750×. Detection of retrograde labeling of ganglion cells was straightforward when microspheres were used as the tracer (see Fig. 3E). In HRP material, ganglion cells in some regions exhibited nonspecific, homogeneous somatic staining, but this was generally faint and easily distinguished from the dark, granular staining typical of retrograde labeling. Alpha cells were distinguished from other ganglion cells on the basis of soma size (Boycott and Wässle, 1974; Wässle et al., 1975; Kolb et al., 1981; Leventhal, 1982; Leventhal et al., 1985). We have made no attempt to use soma size to distinguish between beta cells and other nonalpha cells which, for convenience, we will refer to as "gamma cells," following the common usage of that term (Stone, 1983); we do not intend it to refer to the specific morphological type termed "gamma" by Boycott and Wässle (1974).

Using a hardware/software morphometry system (Neurolucida, MicroBrightfield, Baltimore, MD), we entered into a computer the two-dimensional coordinates of retinal landmarks and of labeled cells. Where possible, we plotted the location of every labeled cell throughout the central retina and within 3–4 mm of the horizontal meridian. Elsewhere, we plotted cells in sample regions 600 × 1,000 μm centered approximately 1–2 mm apart. We excluded data wherever we suspected that the beta cell population may have been incompletely labeled. Sometimes (HRP material only) this was because reductions in staining intensity made it difficult to discriminate the most weakly labeled cells from unlabeled ones; otherwise, it was because the density of labeled cells within a zone of labeling appeared to drop off much more steeply than the density of all ganglion cells. In the HRP experiments, such patterns occurred mainly at the periphery of large zones of retrograde labeling and near the optic disk, while in the bead experiments they occurred at the margins of each small patch of labeling (see Results).

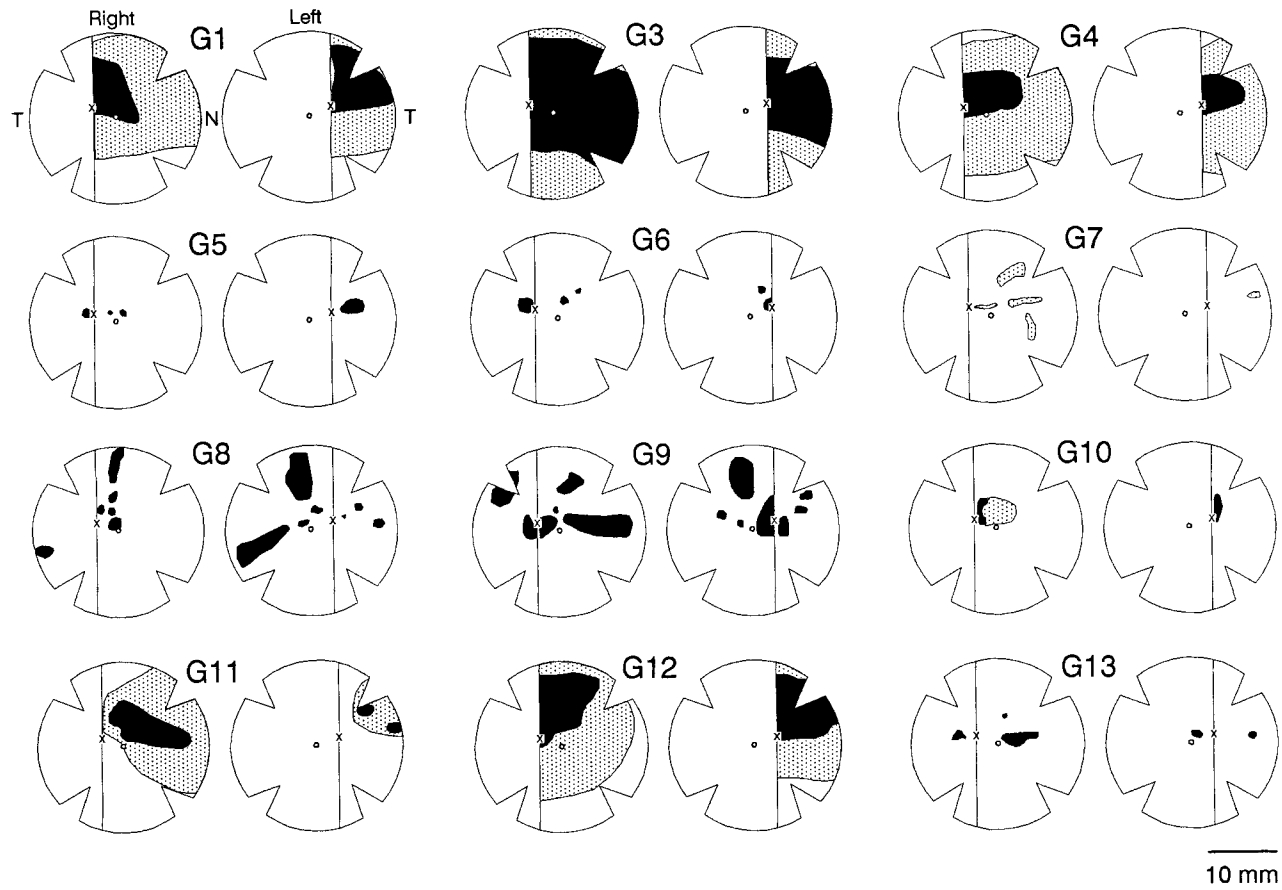

Fig. 1. Schematic summary of distributions of retrograde ganglion cell labeling in these experiments. Data are shown for each animal as a pair of wholemounts displayed roughly in their orientation in situ as viewed by an observer facing the cat: right retina appears to the left, superior is up, nasal is near the midline. Vertical line indicates the zero vertical meridian; x, the area centralis; and o, the optic disk. Black zones represent regions of dense retrograde labeling produced by a saturating tracer injection in the matching region of the geniculate A-layers. Stippled zones show areas of weaker and probably incomplete labeling; such zones were rare among retinas from bead experiments presumably because of limited diffusion of the tracer from the deposit site. In cases of bilateral deposits (cats G5, G6, G8, G9, G13), each LGN injection was assumed to label cells only in the contralateral nasal and ipsilateral temporal retina. N, nasal; T, temporal.

Although inherently subjective, this approach yielded consistent estimates of density among experiments. Estimates of local density were generated by custom software which binned in two dimensions and at selectable resolution the raw data on cell locations. Bins were typically 100 × 100 μm for the central retina and 200 × 200 μm elsewhere. Isodensity contours reflecting local mean density were drawn by eye through the two-dimensional array of local density estimates. For ease of comparison, data have been illustrated except in Figure 1 as if the deposits had been made in the left LGN. No adjustment has been made for retinal shrinkage, which was negligible. We have assumed that one millimeter on the retina equals 4.6 degrees of visual angle. This conversion factor, derived from the mean posterior nodal distance of the cat eye in situ (Vakkur et al., 1963), has been independently shown to apply to wholemounted retinas processed by these methods (Berson and Stein, 1995). The position of the area centralis and axis of the visual streak were typically determined from the local densities of ganglion cells as revealed by retrograde staining. In the HRP experiments, we were also able to exploit the nonspecific background staining of ganglion cells. To localize the area centralis and identify unlabeled ganglion cells in some experiments using fluorescent beads, we counterstained the retina with bisbenzimide or acridine orange (Schmued et al., 1982) or marked all ganglion cells by retrograde transport of biocytin (4% in Tris buffer) applied to the stump of the optic nerve in the eyecup in vitro for one hour (cat G10; Lachica et al., 1991).

Analysis of effective injection sites

Table 1 summarizes the extent of the effective injection site in each experiment. For bead experiments the evaluation was made by direct histological analysis of the circumscribed deposits and corroborated by patterns of retinal labeling (see below). For the HRP studies, in which deposit sites were not sharply defined in the histology, the effective injection zone was inferred primarily from patterns of ganglion cell labeling. The topographic distribution of cell labeling is summarized for each retina in Figure 1. Labeling of alpha and presumed beta cells in the temporal retina was taken to reflect involvement of layer A1. When layer A1 was strongly involved, the appearance of smaller labeled ganglion cells in topographically corresponding zones was taken as evidence for encroachment of the effective deposit

TABLE 1. Summary of Injection Sites

	Tracer	No. of inj.[1]	A[3]	A1	C	MIN	LGNv
G1	HRP	37	***[2]	***	*	**	*
G3	HRP	60	***	***	**	**	**
G4	HRP	64	***	***	*	*	*
G5	Beads	52	*	***	*	—	—
G6L	Beads	15	*	—	—	—	—
G6R	Beads	9	**	**	*	*	—
G7	Beads	28	**	*	—	—	—
G8L	Beads	25	**	**	—	—	—
G8R	Beads	23	**	**	*	—	—
G9L	Beads	19	**	**	*	—	—
G9R	Beads	10	**	**	—	*	—
G10	Beads	44	**	**	—	—	—
G11	HRP	18	**	*	*	—	*
G12	HRP	14	**	**	*	*	—
G13L	Beads	25	**	**	—	—	—
G13R	Beads	12	**	**	—	—	—

[1]Number of separate injection penetrations made.
[2]Extent and intensity of involvement of geniculate divisions, assessed as described in Materials and Methods, indicated by number of asterisks: 3, heavy; 2, moderate; 1, weak; dash, none.
[3]A, A1, C, layers of the dorsal lateral geniculate nucleus; MIN, medial interlaminar nucleus; LGNv, ventral lateral geniculate nucleus. In no experiment did injections involve the optic tract or retinal targets outside the geniculate.

into the underlying geniculate C-layers. The strength of cell labeling near the vertical meridian provided an index of the intensity of involvement of the medial margin of the A-layers and, by extrapolation, of the adjacent medial interlaminar nucleus (MIN). Likewise, labeling at the superior nasal margin of the contralateral retina indicated that the rostrolateral margin of layer A was involved in the deposit and, most likely, the adjacent ventral division of the LGN (LGNv). The contralateral temporal retina was never labeled except within a few hundred microns of the zero vertical meridian; this implies that the effective deposits invariably spared the optic tract and layer 3 of the MIN (Guillery et al., 1980) which contain fibers of contralateral temporal retinal origin.

Intracellular staining of beta cells

We stained ganglion cells by intracellular injection in the living retina in vitro using established methods (Pu and Berson, 1992; Pu et al., 1994). Intracellular dyes consisted of Lucifer Yellow and either biocytin or Neurobiotin. Retinas were superfused at room temperature with oxygenated Ames medium and intracellular impalements made under visual control. In some cases, we tagged ganglion cells by retrograde transport of beads deposited in the A-layers (17 retinas from 9 cats) or in the medial interlaminar nucleus of the LGN (MIN; 5 retinas from 4 cats; see Pu and Berson, 1991). Except for the large alpha cells, bead-labeled cells were targeted for injection irrespective of soma size. In other experiments (5 retinas from 5 cats), we stained retinal neurons supravitally with acridine orange (see Pu et al., 1994 for details) and targeted medium-sized ganglion cells for impalement to maximize the yield of stained beta cells. The topographic distribution of impalements was constrained in the bead experiments to zones of retrograde labeling, predominantly in the visual streak and superior retina. In the acridine-stained retinas, topographic sampling was more or less random though we generally avoided the vicinity of the optic disk where impalements are difficult. Retinas were fixed for 2 hours in 4% buffered paraformaldehyde, processed immunohistochemically (Pu and Berson, 1992), and mounted on glass slides. They were usually coverslipped with an aqueous mountant without prior dehydration or clearing to preserve the microsphere labeling. In some instances, retinas were dehydrated, cleared and coverslipped with Permount; this produced negligible linear shrinkage in the plane of the wholemount (see Pu et al., 1994). Dendritic field measurements were made only in fully stained beta cells. Computer-based systems for mapping (Neurolucida) and perimetry (Sigma Scan, Jandel Scientific, Corte Madera, CA) calculated the area of convex polygons traced around the perimeter of the arbor.

RESULTS

Intraretinal densities of beta cells

Figure 2 shows results from the cat (G3) in which geniculopetal ganglion cells were labeled over the widest retinal extent. The HRP injections were centered in the rostral two-thirds of the A-layers, mainly within the representation of the horizontal meridian and lower visual field. Densities of labeled presumptive beta cells peaked at about 6,100 cells/mm^2 in the area centralis of the contralateral retina (Fig. 1A, right, asterisk) and 6,300 cells/mm^2 in the ipsilateral retina (Fig. 1A, left). These values probably underestimate beta cell densities at the area centralis. Ipsilaterally and contralaterally projecting beta cells intermingle at the nasotemporal raphe (Stone, 1983), so the unilateral geniculate deposit presumably left some beta cells in each eye unlabeled in the zone of overlap, which includes the area centralis. Outside the central retina, isodensity contours showed a marked horizontal elongation, especially nasally, corresponding to the visual streak. Within a millimeter of the area centralis there were no obvious nasotemporal differences in density, but more peripherally nasal densities exceeded temporal ones, especially in the visual streak.

The core of the histologically visible deposit in this experiment lay mainly within the A-layers (Fig. 2B, black zones, and Fig. 3A). Weaker staining (stippling) also reached the C-layers, the underlying optic tract, the MIN and LGNv. The topography of retinal labeling (Fig. 1) indicates that the deposit may have been at least partly effective in some of these (see Materials and Methods and Table 1). However, involvement of structures beyond the A-layers seems to have had little impact on the labeling patterns. The size distribution of labeled somas closely resembled those in experiments with tracer injections clearly limited to the A-layers (cf. Fig. 11; see also Stone and Keens, 1980; Leventhal et al., 1985). The smallest ganglion cells (i.e., smaller than beta cells) should have been labeled in substantial numbers had the effective deposit involved the optic tract, pretectum, or LGNv (Leventhal et al., 1985), but they were not. When small ganglion cells were encountered (Fig. 3B and C, arrowheads), they usually lay within the most intensely labeled retinal zones, corresponding retinotopically to the pipette tracks in the LGN. This pattern suggests that the small cell labeling was produced by the spread of some deposits into the underlying C-layers (Leventhal et al., 1985), which lie in topographic register with the A-layers, rather than into the MIN, LGNv, or optic tract. Additional evidence will be provided below that any spread of the effective deposit beyond the A-layers had little impact on the estimates of beta cell density.

Figure 4 illustrates results in a cat (G4) with a much smaller geniculate HRP deposit and less involvement of the MIN and LGNv. Labeled small gamma cells were even less frequently labeled than in the first cat and appeared confined to retinal regions with intense ganglion cell labeling, suggesting localized involvement of the C-layers. The

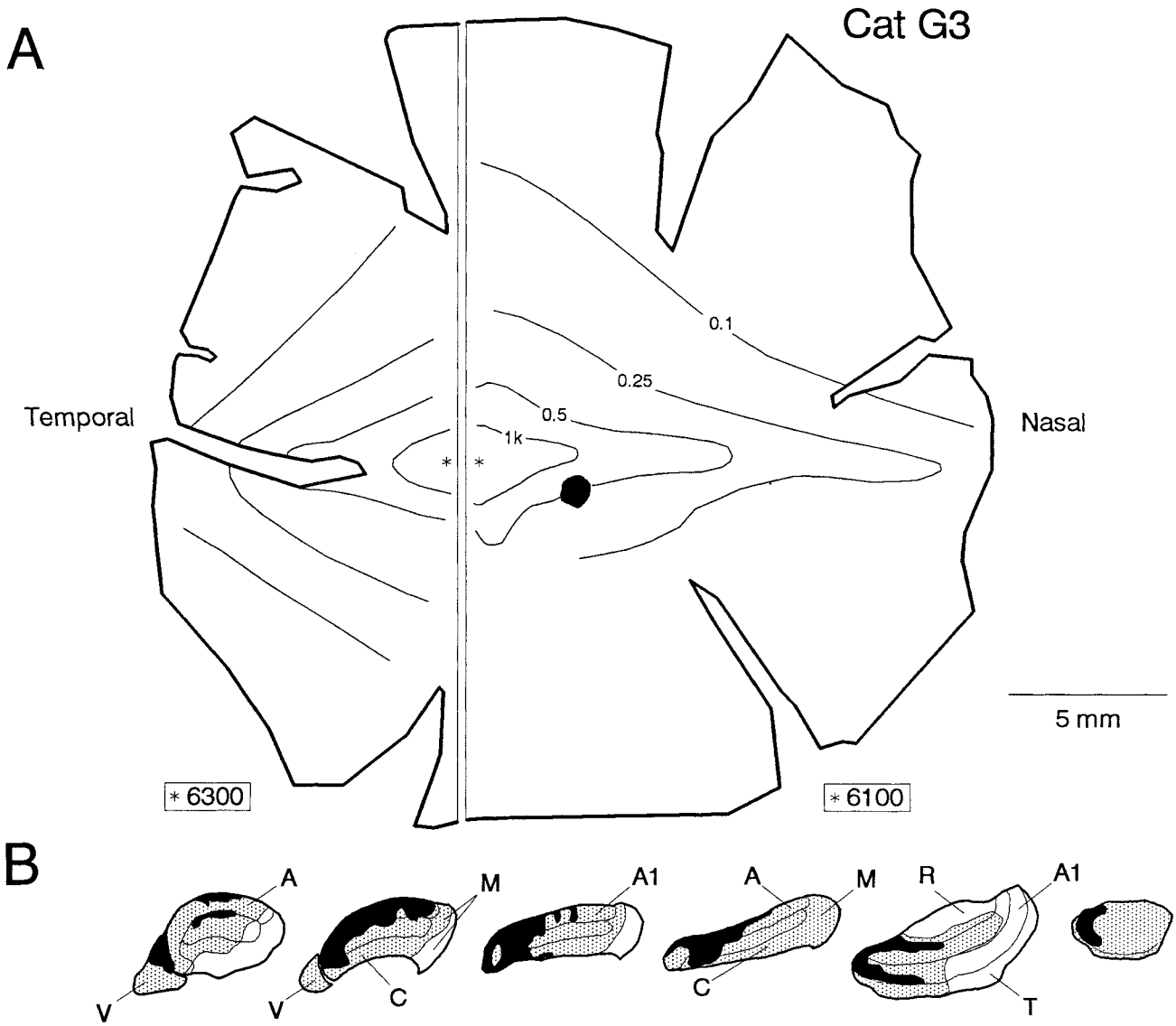

Fig. 2. Estimated distribution of retinal beta cells as inferred by patterns of retrograde labeling after deposits of horseradish peroxidase into the A-layers of the lateral geniculate nucleus (cat G3). **A:** Distribution of presumed beta cells in the nasal retina contralateral (right) and temporal retina ipsilateral (left) to the thalamic deposit. The ipsilateral temporal hemiretina has been reflected about the nasotemporal raphe and apposed to the contralateral nasal hemiretina to simulate the beta cell distribution within a single retina. The two hemiretinae not shown were devoid of beta cell labeling. Asterisks represent the area centralis, the site of peak density: 6,100 cells/mm^2 for the contralateral nasal retina and 6,300 cells/mm^2 for the ipsilateral temporal retina (boxes at bottom). Black spot in the nasal hemiretina is the optic disk. Cells were presumed to be beta cells if they were labeled by retrograde transport and too small to be alpha cells. A few of these cells were probably gamma cells labeled by spread of the deposit to geniculate compartments beyond the A-layers (see text for details). Isodensity contours labeled in thousands of cells/mm^2; contours have been truncated in regions where retrograde labeling appeared submaximal. **B:** Histological appearance of the injection site illustrated in tracings of representative frontal sections. Section at left is most rostral, that at right is most caudal. Black zones indicate densest deposit and stippled zones areas of weaker staining. Appearance of the deposit may not accurately reflect the extent of the effective injection (see text). A, layer A; A1, layer A1; C, C-layers; M, medial interlaminar nucleus; R, optic radiations; T, optic tract; V, ventral division of lateral geniculate nucleus.

distribution of presumed beta cells had much the same form as in that in the first experiment (Fig. 2), including a prominent visual streak and generally higher densities nasally than temporally. The estimates of beta cell density were among the lowest in the present study. The peak density in the contralateral area centralis (5,600 cells/mm^2) was nearly as high as in cat G3 (Fig. 2), but elsewhere densities were typically about 30% lower. Densities reached a peak in the ipsilateral area centralis of 4,000 cells/mm^2.

The three other HRP cases provided similar results (cats G1, G11, and G12; Fig. 5). The deposits in all three cases were centered in layer A and may have involved the C-layers; in two of the three cases (G1, G12) deposits may have encroached into the MIN, and in two (G1, G11), may have involved the LGNv (Table 1). Estimated beta cell densities were always within the range of those at matched locations in the first two experiments (Figs. 2 and 4), and were typically intermediate between them, although in one

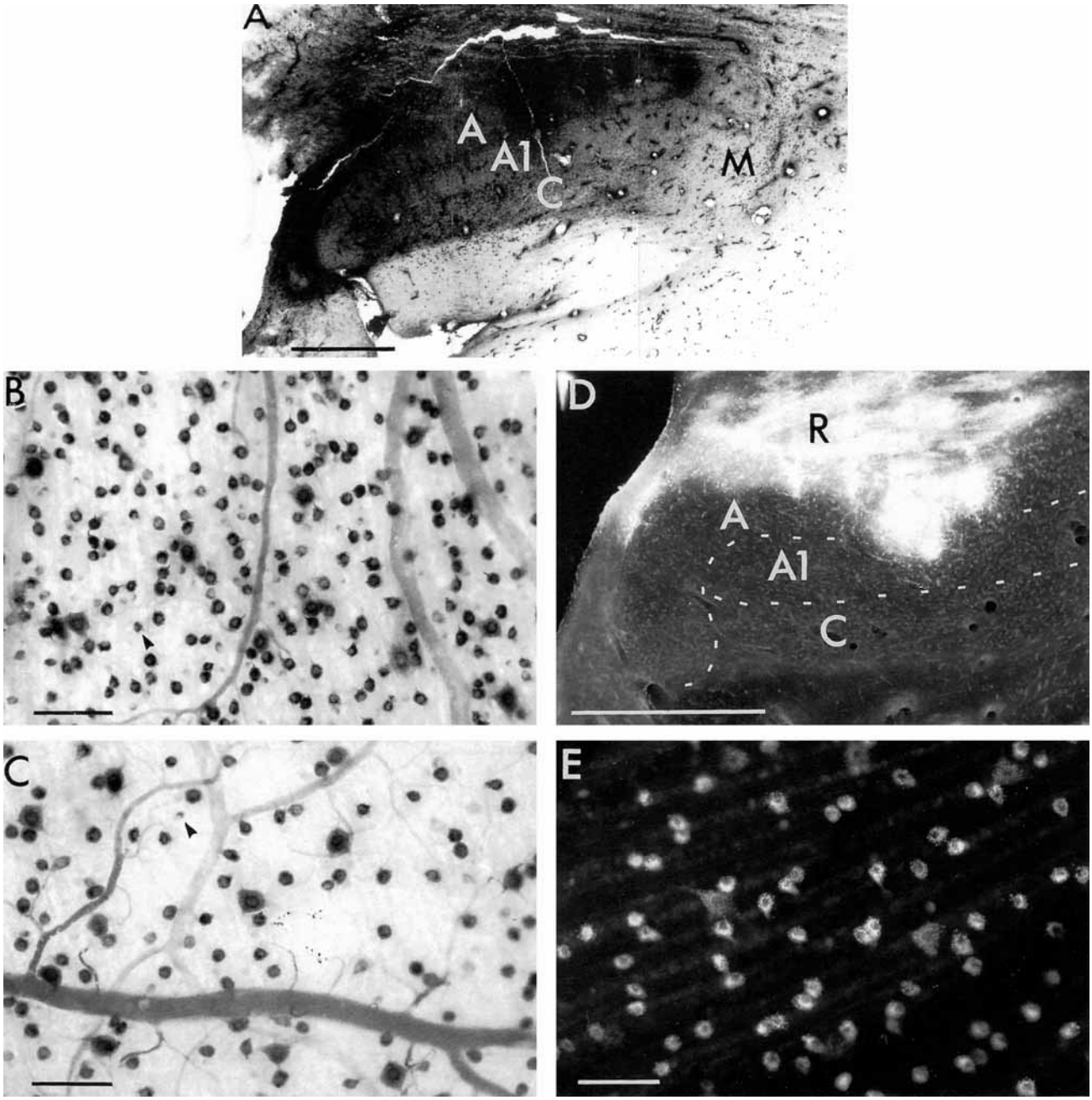

Fig. 3. Photomicrographs illustrating thalamic deposits and patterns of retinal labeling in two experiments, one with horseradish peroxidase (HRP; A–C) and another with beads (D,E). **A:** Photomontage showing appearance of HRP injection site in cat G3. **B,C:** Pattern of retrograde HRP labeling of ganglion cells at two sites in the contralateral nasal retina of cat G3. Except for the large alpha cells, and a very few small presumed gamma cells (arrowheads), nearly all of the labeled cells had intermediate soma sizes typical of beta cells. Many of the smallest ganglion cells exhibit faint homogeneous staining not indicative of retrograde labeling. The fields shown in B and C lay at comparable eccentricities (5.0 mm in B; 4.7 mm in C), but B lay within the visual streak while C lay 3.2 mm superior to it. Within the streak (B), the density of presumed beta cells (i.e., labeled nonalpha cells) was clearly higher and soma size was smaller on average than outside the streak (C; see text for details). **D:** Fluorescence photomicrograph of bead deposits in cat G13L. Note that deposit is confined to geniculate A-layers. **E:** Fluorescence photomicrograph of retrograde bead labeling in contralateral retina of cat G13L (6 mm eccentricity near visual streak). Scale bars: 1 mm for A and D; 100 μm for B, C, and E. A, A1, C, layers of LGN; M, medial interlaminar nucleus; R, optic radiations.

cat (G1) they usually equalled the maximal values in cat G3 (Fig. 1). All three experiments clearly confirmed the horizontal elongation of isodensity contours in the nasal periphery. Two of them yielded good cell labeling in the central retina and confirmed the earlier findings there. In cat G1, estimated beta cell density reached a peak of 5,600 cells/mm^2 in the middle of the contralateral area centralis (cf. 6,100 cells/mm^2 in G3 and 5,600 cells/mm^2 in G4). Cat G12

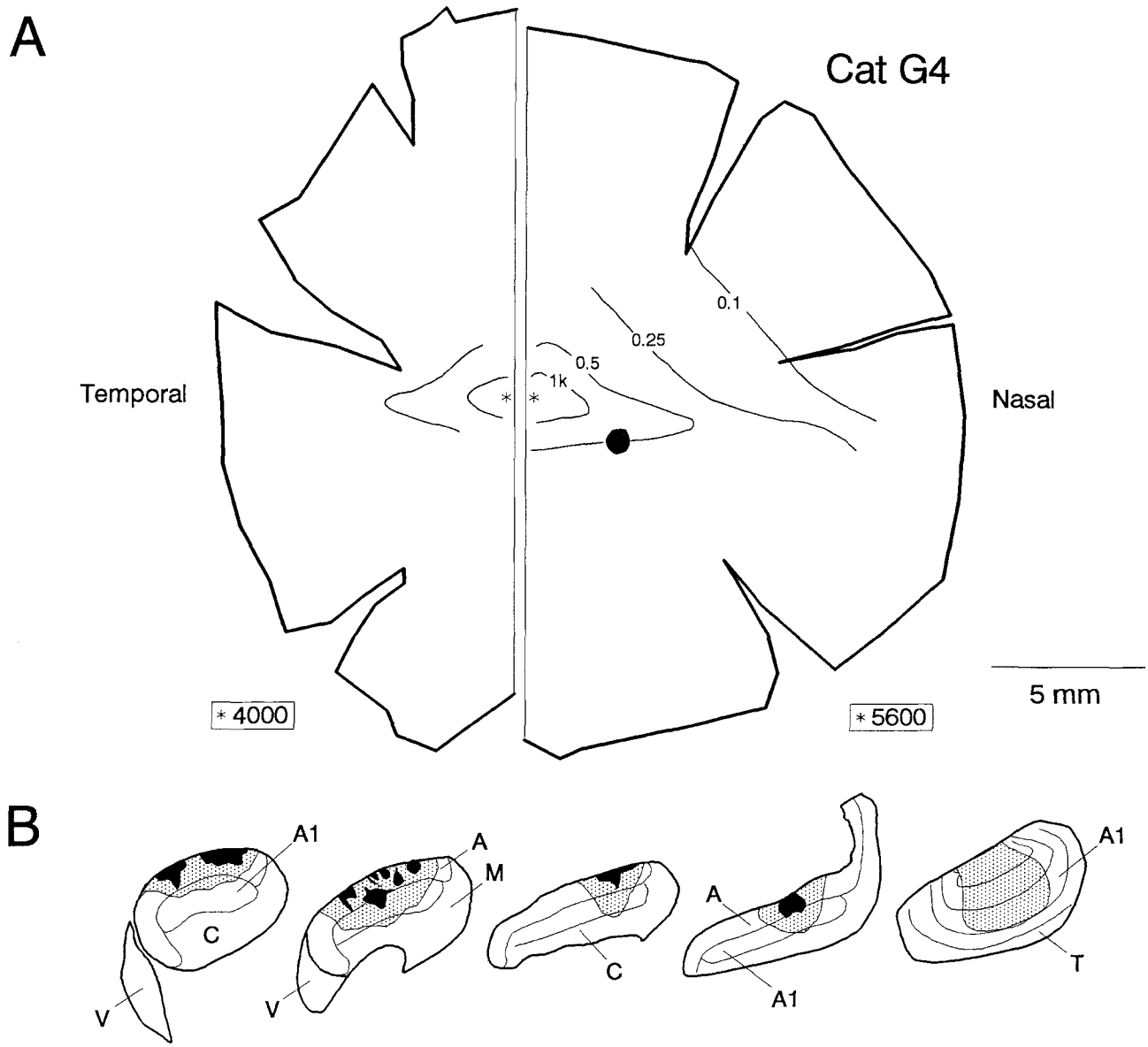

Fig. 4. Estimated distribution of retinal beta cells as inferred in cat G4 by retrograde transport of horseradish peroxidase from the geniculate. **A:** Isodensity maps of presumed beta cells in the contralateral nasal (right) and ipsilateral temporal (left) hemiretinas. Peak densities at the area centralis (asterisks) shown in boxes below. **B:** Injection site (may not reflect the extent of the effective injection). Conventions and abbreviations as in Figure 2.

lacked labeling in the middle of the area centralis but 200 μm nasal to it densities reached 4,100 cells/mm^2, at least as high as the matching values in cats G3 and G4.

The experiments using latex beads confirmed the HRP findings, although the compact deposit sites (Fig. 3D) kept the zones of retinal labeling small (Fig. 1) and precluded complete mapping of the beta cell topography. Estimated beta cell densities were within the range observed in the HRP experiments except in cat G7, in which injections were unusually small and widely spaced and may have left some beta cells unlabeled. In the later bead experiments (G9L, G9R, G10, G13L, and G13R), in which we tightly clustered the deposits, beta cell densities typically approached or exceeded the maximal values in the HRP studies (cf. Figs. 2, 6 and 9). *This was true throughout the retina* and despite the fact that the deposits were virtually restricted to the A-layers: other geniculate divisions were entirely spared in most cases (G10, G13R, G13L) and their minimal involvement in the others (G9L, G9R) could be discounted on topographic grounds. For example, in the pericentral retina (eccentricities 300–600 μm), estimated beta cell densities were at least as high in the bead experiments (cats G9L, G9R, G10) as in the HRP studies, even when the bead deposits were unequivocally restricted to the A-layers (cat 9L, Fig. 6; cat G10, Figs. 9 and 10A). Beta cell densities were higher in the nasal visual streak than at matched eccentricities in the nonstreak periphery in all four bead experiments examined (G8L, G8R, G9L, G13L), including two with injections effectively restricted to the A-layers (Figs. 6, 9, 10C,D). In the temporal retina, four bead

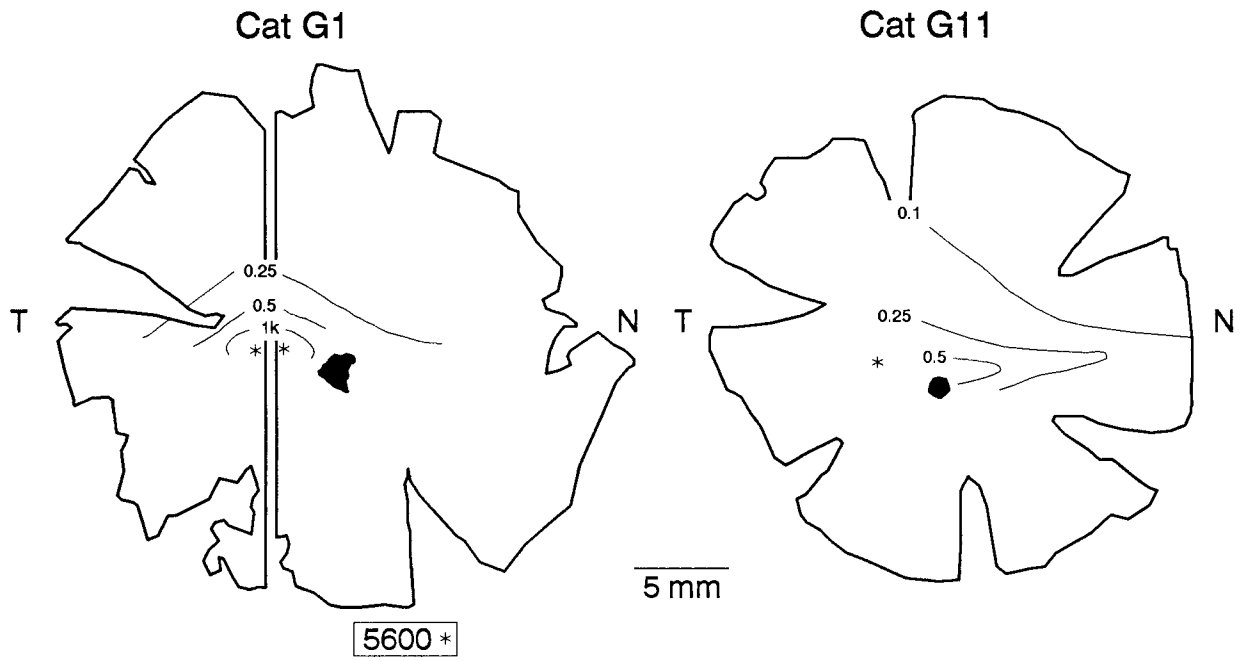

Fig. 5. Estimated distribution of retinal beta cells in two additional animals, cats G1 (left) and G11 (right), as inferred by retrograde transport of horseradish peroxidase from the geniculate. Conventions and abbreviations as in Figure 2; asterisks indicate area centralis. Densities of presumed beta cells at the area centralis reached 5,600 cells/mm^2 in the contralateral retina of G1; labeling of central retina was absent in G11 and too weak in the ipsilateral eye of G1 to permit density estimates there. Data from the ipsilateral temporal retina in G11 were too fragmentary to permit reconstruction of isodensity contours.

experiments (G5, G9R, G13R, and G13L), including two with injections restricted to the A-layers (G13L and G13R), gave estimated beta cell densities approaching the maximal values from the HRP studies. Other bead experiments typically exhibited lower temporal densities, probably because layer A1 was not heavily involved in these deposit sites as reflected by the limited extent of temporal labeling (Fig. 1).

In five experiments in which the bead injections were largely or completely confined to the A-layers (G7, G8R, G8L, G9R, G9L), we used intracellular injection in vitro to stain more than 300 bead-labeled nonalpha cells. Virtually all of these exhibited beta cell morphology except for a handful at retinal locations topographically related to circumscribed encroachment of deposits into the C-layers or MIN. This supports the assumption that, except for alpha cells, only beta cells innervate the geniculate A-layers.

Fractional contribution of beta cells to the ganglion cell population

The fraction of all ganglion cells that are beta cells varies over the retina. Figures 7 and 8 document a series of local comparisons of estimated beta cell densities in a single HRP experiment (G3) with total ganglion cell densities derived from a separate Nissl-stained retina. Figure 7 evaluates the beta cell fraction along the nasotemporal axis. Figure 7A plots local densities of beta cells (triangles) and all ganglion cells (squares) along a horizontal traverse aligned with the nasal visual streak and passing through the area centralis (see inset). Also plotted for comparison are densities of alpha cells in the Nissl-stained retina (open circles) as well as densities of gamma cells (filled circles) as estimated in our study of colliculopetal ganglion cells (Stein and Berson, 1995). All cell classes exhibited a clear peak in density in the central retina, but this appeared more prominent for the beta cells than for other ganglion cells. Beta cells appeared to outnumber the other classes not only centrally but in the temporal retina as well. These points are emphasized in Figure 7B, which plots the estimated fraction of all ganglion cells belonging to each of these classes. Beta cells (triangles) account for about half of all ganglion cells in the peripheral nasal retina, but this fraction rises to about two-thirds in the area centralis and temporal retina. Gamma cells (filled circles) undergo a complementary decrease in relative numbers, from about half of the ganglion cells of the nasal periphery to roughly a third of those in the temporal periphery. The upper solid line ("Sum") plots the sum of the estimated alpha, beta, and gamma fractions. This comes close to 100% at all eccentricities. In other words, along the entire traverse the sum of the estimated densities of the component populations closely matched the density of all ganglion cells in the Nissl-stained retina.

Figure 8 assesses the relative contributions of beta and other ganglion cells to the nasal visual streak by comparing their densities along an arc of isoeccentricity (7.3 mm or 33 degrees from the area centralis). As shown in Figure 8A, beta cells (triangles) exhibited a maximum in density at the nasal visual streak that was as prominent as that for gamma cells (filled circles). This is confirmed in Figure 8B, which replots the densities of these ganglion cell classes as a fraction of the total ganglion cell density in the Nissl-stained retina. Beta and gamma cells each make up about 45–50% of all ganglion cells in the streak, just as they do elsewhere in the nasal retina at this eccentricity.

Although the foregoing analysis relied on comparisons of retinas from several different animals, the central conclu-

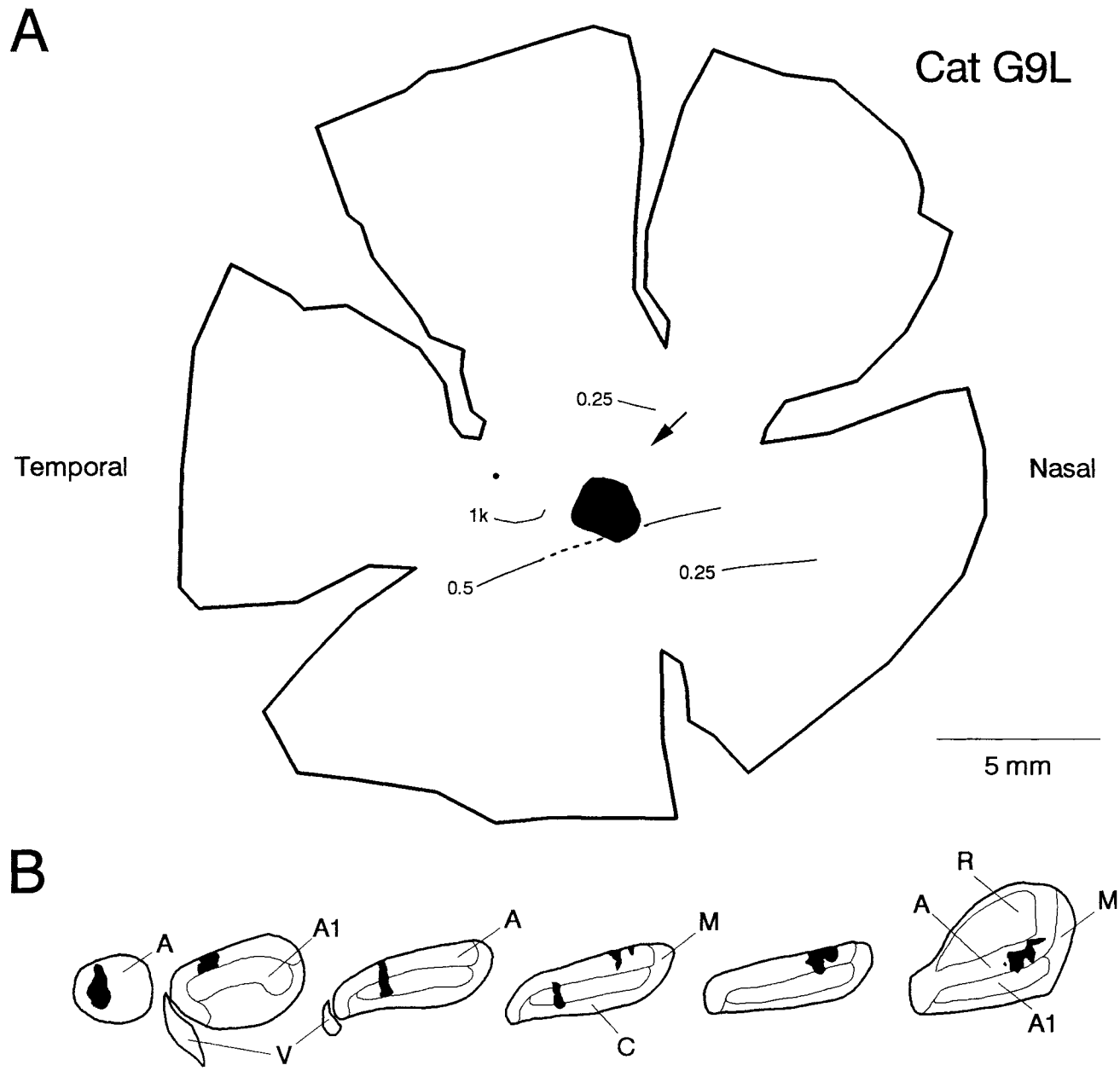

Fig. 6. Estimates of beta cell density as inferred by patterns of retrograde transport of fluorescent latex beads into the A-layers of the lateral geniculate nucleus (cat G9L). **A:** Distribution of presumed beta cells in contralateral nasal retina. **B:** Injection sites. Conventions and abbreviations as in Figure 2. Zone of retrograde labeling did not include the area centralis (dot in A), but peak densities of presumed beta cells reached 2,700 cells/mm^2 at an eccentricity of 600 μm, a value matching that at a comparable location in cat G3 (Fig. 2) and slightly higher than that in cat G4 (Fig. 4). Limited tracer diffusion made for clearly defined injection sites (black zones in B) and relatively small zones of retinal labeling (Fig. 1) that permitted only partial reconstruction of the beta cell distribution. The deposits were entirely confined to the A-layers except for a circumscribed encroachment into the upper C-layers (middle two sections in B). Arrow in A marks the site corresponding retinotopically to this C-layer injection site as inferred from multiunit recordings. Densities within a millimeter of this retinal location were excluded from the analysis. A few bead-labeled cells in this region had nonalpha and nonbeta morphology as revealed by intracellular staining, but elsewhere all 47 cells stained had beta morphology.

sions appear robust. For example, the densities plotted for beta and gamma cells were corroborated in other experiments (present study; Stein and Berson, 1995) and those for alpha cells and all ganglion cells are consistent with earlier reports when appropriate corrections are made for differential shrinkage (e.g., Wässle et al., 1975; Wong and Hughes, 1987). Moreover, we confirmed the major findings by comparing within single retinas the densities of beta cells with those of other ganglion cells (Figs. 9 and 10; 9 sites in three experiments). Beta cells were identified by retrograde bead labeling after deposits entirely restricted to the A-layers and other ganglion cells by retrograde bulk filling (cat G10) or Nissl staining (G13R and G13L). In agreement with the initial analysis (Figs. 7 and 8), beta cells

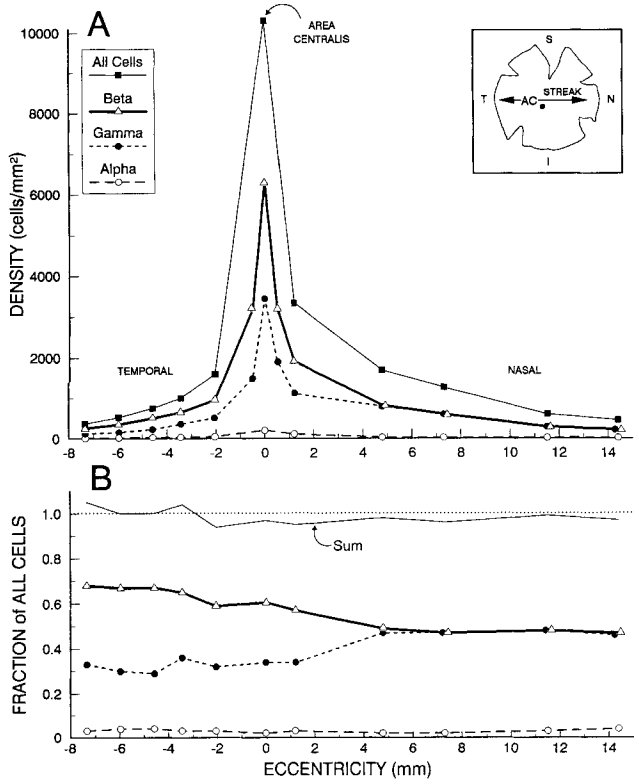

Fig. 7. Comparison of estimated local densities of beta cells with those of other ganglion cells along the nasotemporal axis of the retina. The sampling traverse (double-headed arrow in **inset**), was aligned with the visual streak of the nasal retina. Ganglion cell densities were estimated from the following sources: beta cells (triangles), cat G3 (Fig. 1); all ganglion cells (squares) and alpha cells (open circles), cat N1; and gamma cells (filled circles), cat F2. Linear shrinkage was negligible in all retinas. In cat N1, ganglion cell densities were derived from cell counts in the ganglion cell layer after staining with bisbenzimide; amacrine cells were excluded and alpha cells were identified on the basis of soma size. In cat F2, gamma cells were identified by selective retrograde HRP labeling from the superior colliculus, to which virtually all gamma cells apparently project (Stein and Berson, 1995); alpha cells were excluded on the basis of soma size; densities in temporal retina represent the sum of ipsilaterally and contralaterally projecting populations. See Stein and Berson (1995) for further details on cats N1 and F2. **A:** Ganglion cell densities as a function of distance from the area centralis. AC, area centralis; I, inferior; N, nasal; S, superior; T, temporal. **B:** Estimated proportions of ganglion cell population belonging to the beta, gamma, and alpha classes. Fractions were estimated for each class by dividing density for that class by total ganglion cell density as estimated from the Nissl-stained retina (N1). Beta cells represent roughly half of all ganglion cells in the peripheral nasal retina, at least 60% of the ganglion cell population at the area centralis and about two-thirds in the temporal retina. Beta cell densities and fractions are probably underestimated somewhat at the area centralis which lies in the zone of nasotemporal overlap (see text). Upper solid line ("sum") represents sum of the beta, gamma, and alpha cell fractions. This lies close to the line of unity (dotted horizontal line) at nearly all eccentricities, supporting the validity of the analysis (see text).

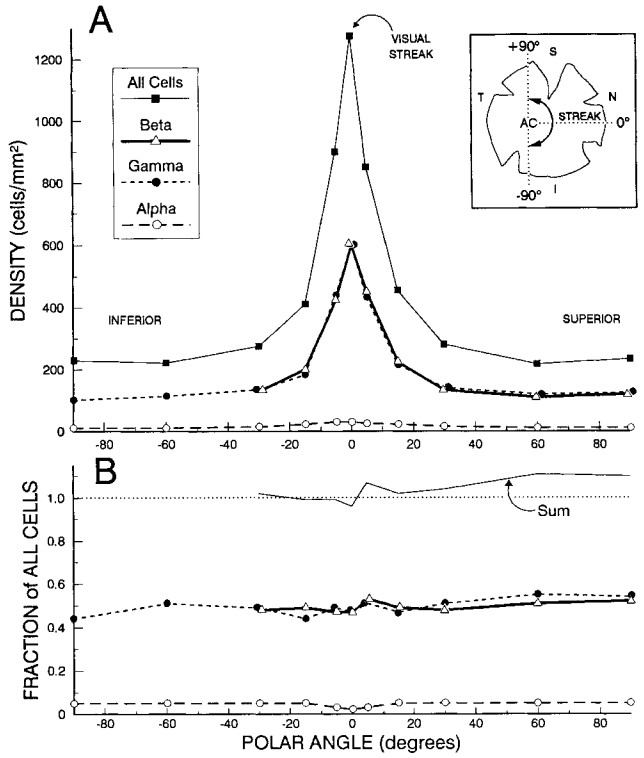

Fig. 8. Relative contribution of beta and other ganglion cells to the nasal visual streak. Local density and fractional contribution are evaluated along a semicircular isoeccentricity traverse lying 33 degrees (7.3 mm) from the area centralis in the nasal retina (see **inset** in A). Sources for data and conventions same as for Figure 7. **A:** Estimated densities along the arc. Abscissa plots polar angle along the traverse where 0 degrees represents the intersection of the traverse with the nasal visual streak and positive angles lie in the superior retina. AC, area centralis; I, inferior; N, nasal; S, superior; T, temporal. **B:** Fraction of all ganglion cells that are beta, gamma, and alpha cells as a function of position along the sampling arc. Beta cells appear to be as highly concentrated in the visual streak as are other ganglion cells.

accounted for 60–67% of the ganglion cells in the central and temporal retina, but only about half of those nasally, whether within or outside the visual streak.

Alpha cells represent the same fraction of all ganglion cells in the nasal as in the temporal periphery (Wässle et al., 1975; Hughes, 1981b), so the proposed elevation of the beta cell fraction in the temporal retina predicts relatively higher ratios of beta to alpha cells there as compared with the nasal periphery. This proved to be the case. Beta:alpha ratios were 60% higher in the temporal periphery (mean = 14.4; range 12:1–16:1; n = 7 in 4 cats) than in the nasal periphery (mean = 9.1; range 6:1–15:1; n = 15 in the same 4 cats). Elevation of the beta cell fraction temporally also predicts that the distribution of beta cells should be more symmetric about the nasotemporal raphe than is the nasally biased distribution of all ganglion cells. This prediction too is confirmed. For example, in maps of total ganglion cell density (Rowe and Stone, 1976; Hughes, 1981b; Wong and Hughes, 1987), temporal densities are roughly 35–50% those at matched eccentricities nasally (4–6 mm horizontal eccentricity). In the three experiments in which we could make a matched comparison (cats G3, G4, G11), temporal beta cell densities were 65–90% of those nasally.

One observation that has been offered as evidence for decreased beta cell incidence in the visual streak is that small (presumptive gamma) ganglion cells are disproportionately concentrated there (Rowe and Stone, 1976; Stone and Keens, 1980). However, an alternative interpretation of that finding is that beta cells undergo reductions in soma size in the streak and thus contribute to the population of "small" ganglion cells there (Hughes, 1981b). Our data

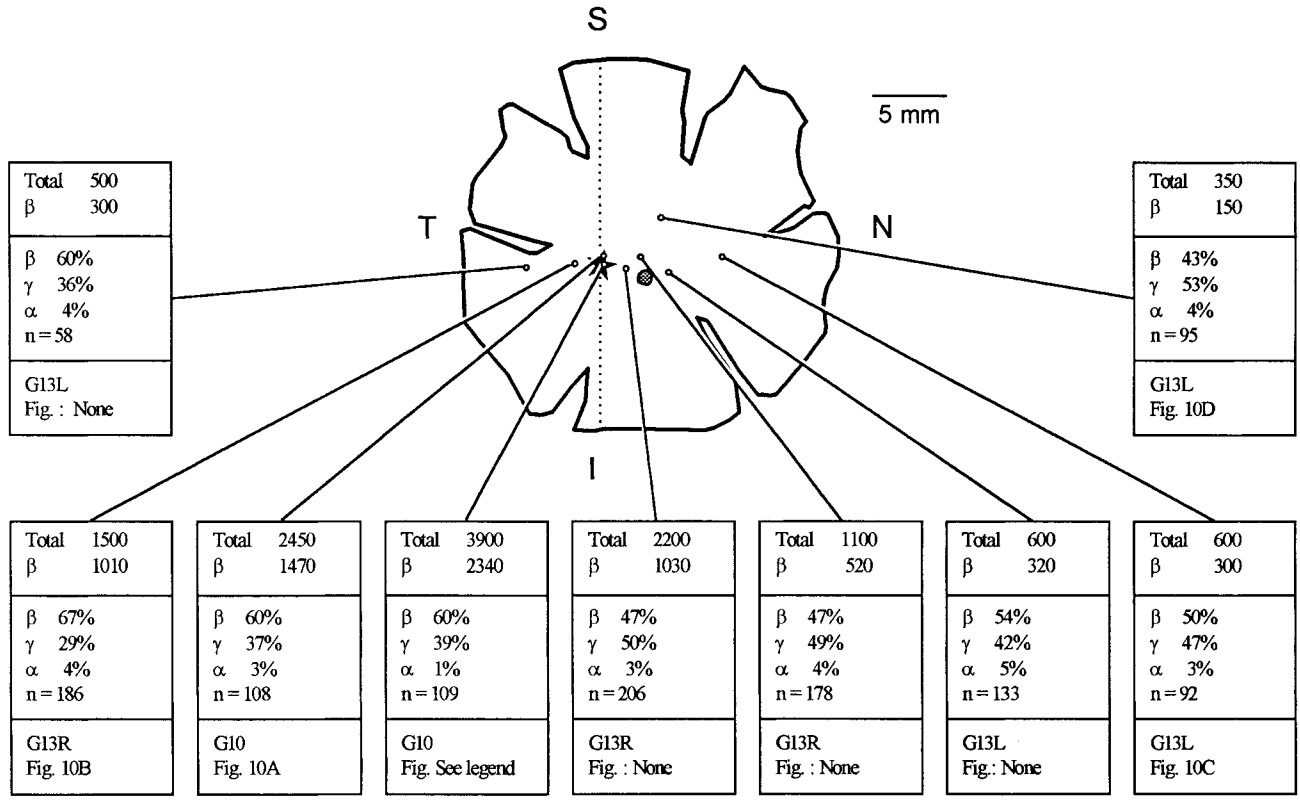

Fig. 9. Topographic variations in the beta cell fraction as revealed by direct comparisons of densities of labeled beta cells with those of other ganglion cells in single retinas. In central schematic retina, star represents the area centralis, shaded circle the optic disk, and dotted line the vertical meridian. Open circles mark nine sample sites in three retinas labeled by bead deposits restricted to the A-layers. In the box linked to each site, top panel compares the densities (in cells/mm^2) of all ganglion cells as revealed by counterstaining or bulk filling ("Total") with those of bead-labeled beta cells. Middle panel shows the percentage of cells at that site that are beta, gamma or alpha cells as well as the total number of ganglion cells in the sampled zone. Alpha cells were identified on the basis of soma size; the gamma cell group includes all unlabeled nonalpha cells. Bottom panel identifies the experiment from which the sample was obtained and other figures illustrating that site. The sample site nearest the area centralis (from cat G10) is illustrated in Figure 2B of Stein and Berson (1995). I, inferior; N, nasal; S, superior; T, temporal.

support the latter view. For example, bead-labeled presumptive beta cells (filled bars in Fig. 11; cat G13L) were smaller on average within the visual streak (16.5 μm diam ± 0.2 S.E.M.; range 13–20 μm; n = 47; Fig. 11A) than at matching eccentricities elsewhere in the nasal retina (18.8 ± 0.4 μm diam S.E.M.; range 12–26 μm; n = 48; Fig. 11B). Comparable within-retina differences in mean (as well as minimum) beta cell soma size were evident in both HRP cases tested (cat G3, Streak: mean = 17.2 ± 0.2 μm S.E.M., range 14–20 μm, n = 50; nonstreak: mean = 20.8 ± 0.2 μm S.E.M., range 17–25 μm, n = 50; eccentricity 5 mm; from regions shown in Fig. 3B and C. Cat G11, streak: mean = 14.9 ± 0.3 μm S.E.M., range 13–17 μm, n = 20; nonstreak: mean = 17.9 ± 0.4 μm S.E.M., range 15–22 μm, n = 20; eccentricity: 8–9 mm) and in the one case examined in which all the beta cells were morphologically identified by intracellular staining (cat G8R streak: mean = 19.0 ± 0.8 μm S.E.M., range 16–23 μm, n = 10; nonstreak: mean = 25.7 ± 0.8 μm S.E.M., range 20–30 μm, n = 14; eccentricity: 7–10 mm; sample areas in boxes in Figure 12).

Dendritic field dimensions of beta cells

To determine whether beta cell dendritic field sizes are inversely related to beta cell density, we stained 587 beta cells in 27 retinas from 18 cats. Figure 12 illustrates topographic variations in beta cell dendritic profiles stained in a single representative retina. As expected from earlier work (Boycott and Wässle, 1974; Kolb et al., 1981; Dann et al., 1988), beta cell dendritic field dimensions were strongly correlated with retinal eccentricity, being much smaller near the area centralis than in the nasal periphery. In addition, however, they were consistently smaller in and near the visual streak than at matched eccentricities outside the streak. Camera lucida drawings of some of these cells are shown in Figure 13. The three cells with small dendritic fields (top) were located near the axis of the visual streak (lower box in Fig. 12), whereas the two cells with larger dendritic fields were located about 5 mm superior to it (upper box in Fig. 12). Although equidistant from the area centralis (6–7 mm), the cells within the streak had dendritic fields 3- to 4-fold smaller in area than those from the nonstreak site.

To examine this relationship for the entire population of stained beta cells, we divided them into three groups: "streak" cells (< 5 degrees or 1.1 mm from the axis of the nasal visual streak); "nonstreak" cells (> 15 degrees from that axis); and "intermediate" (all others). Figure 14 plots beta cell dendritic field areas as function of retinal eccentricity. In addition to the dependence on eccentricity, there was a systematic effect of proximity to the visual streak. In the

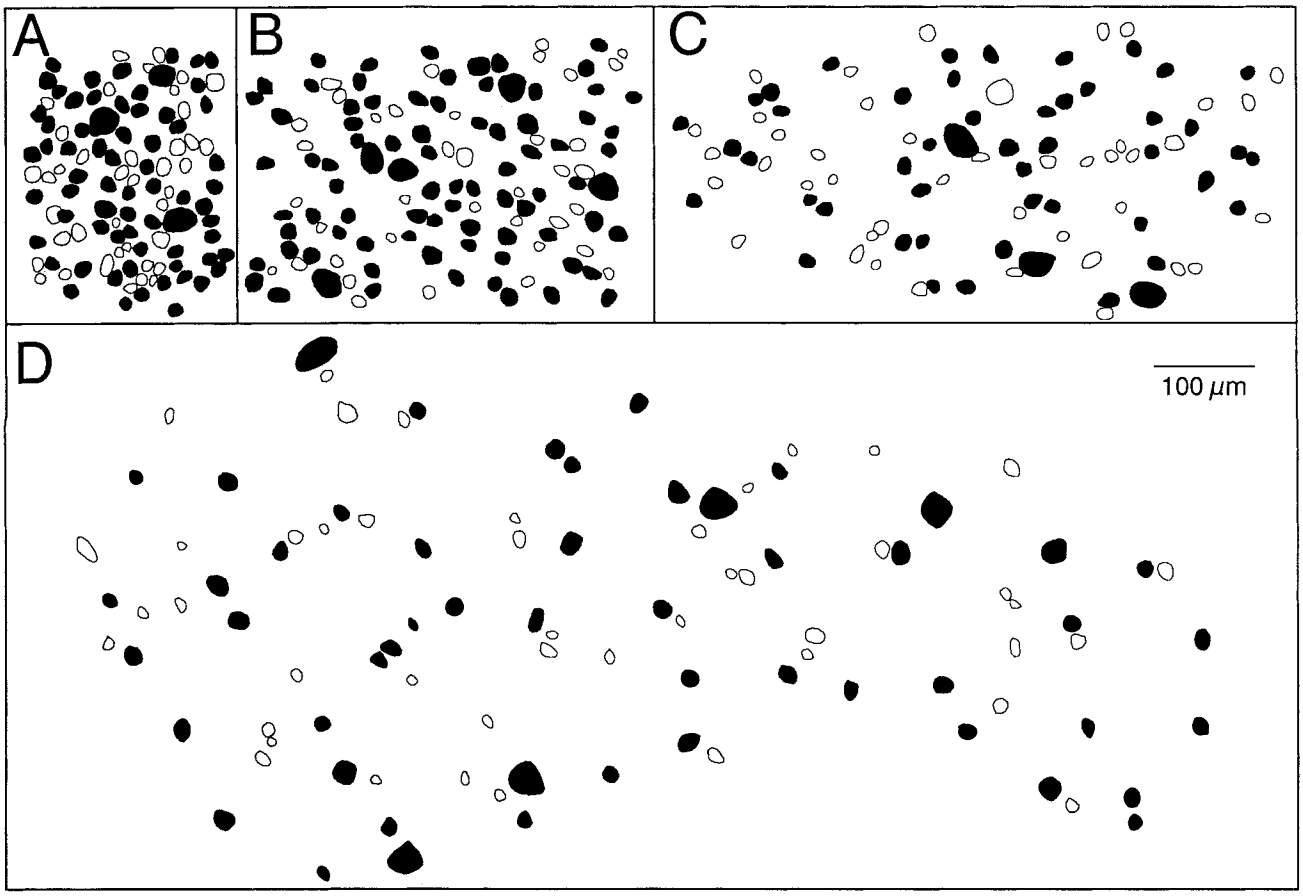

Fig. 10. Topographic variations in beta cell density and fraction. Camera lucida drawings illustrate ganglion cell somas labeled (solid profiles) or unlabeled (open profiles) after bead deposits restricted to the geniculate A-layers. Excluding the large alpha cells, virtually all labeled somas may be presumed to be beta cells and unlabeled ones to be gamma cells. **A:** Central retina (about 700 μm eccentricity; cat G10). **B:** Temporal retina (about 2 mm eccentricity; cat G13R). **C:** Nasal visual streak (8 mm eccentricity; cat G13L). **D:** Nasal nonstreak retina (5 mm eccentricity, 3 mm superior to the streak axis; cat G13L). The streak site (C) has a much higher density of beta cells than the nonstreak site in the same retina (D) even though it lies farther from the area centralis. Labeled beta cells outnumber unlabeled gamma cells in the central and temporal retina (A,B) but are about as common as gammas in the nasal periphery (C,D). See Figure 9 for quantitative analysis of these fractions and location of depicted zones.

nasal retina, dendritic fields of streak cells (open circles) were roughly threefold smaller in area than those of nonstreak cells (filled triangles), with virtually no overlap between the populations. Intermediate cells (not shown for clarity) had intermediate dendritic field areas. In the temporal retina, a similar trend was apparent, although the data were less complete and there appeared to be more overlap. Figure 14 also shows that there is relatively little nasotemporal difference in dendritic field size at matched eccentricities.

Coverage

To determine if beta cell anatomical coverage factor remains constant across the retina, we multipled dendritic field area by local beta cell density for 204 beta cells. Each cell was stained by intracellular injection and lay in a zone of retrograde labeling produced by a latex bead deposit largely or completely restricted to the LGN A-layers. Figure 15 plots these coverage factor estimates as a function of eccentricity. Coverage was essentially constant. It averaged about 4 (mean = 3.93 ± 0.76 S.D.) and was independent of eccentricity and nasotemporal location. It was essentially the same for cells lying within the streak (open circles) as for those in nonstreak (triangles) and intermediate locations (squares), despite 100-fold variations in local beta cell density and dendritic field area.

A map of the beta cell distribution derived from dendritic field dimensions

If beta cell coverage factor is topographically invariant, one can use dendritic field dimensions to probe local beta cell density. Following this logic, we generated 587 local estimates of beta cell density by dividing the dendritic field areas of beta cells at known retinotopic locations into 3.93, an estimate of the coverage constant (see above). Figure 16 illustrates an isodensity map generated from retinotopic plots of such estimates. This map had the same form as those generated from retrograde labeling data, with a prominent visual streak and a sharp increase in density in the area centralis, where peak densities reached 7,000 cells/mm^2 or more. In the temporal retina, densities approached the maximal values obtained in the retrograde tracing experiments, while in the nasal periphery they were somewhat lower, comparable to those in cat G4 (Fig. 4). The calculated densities depend critically on the value used for

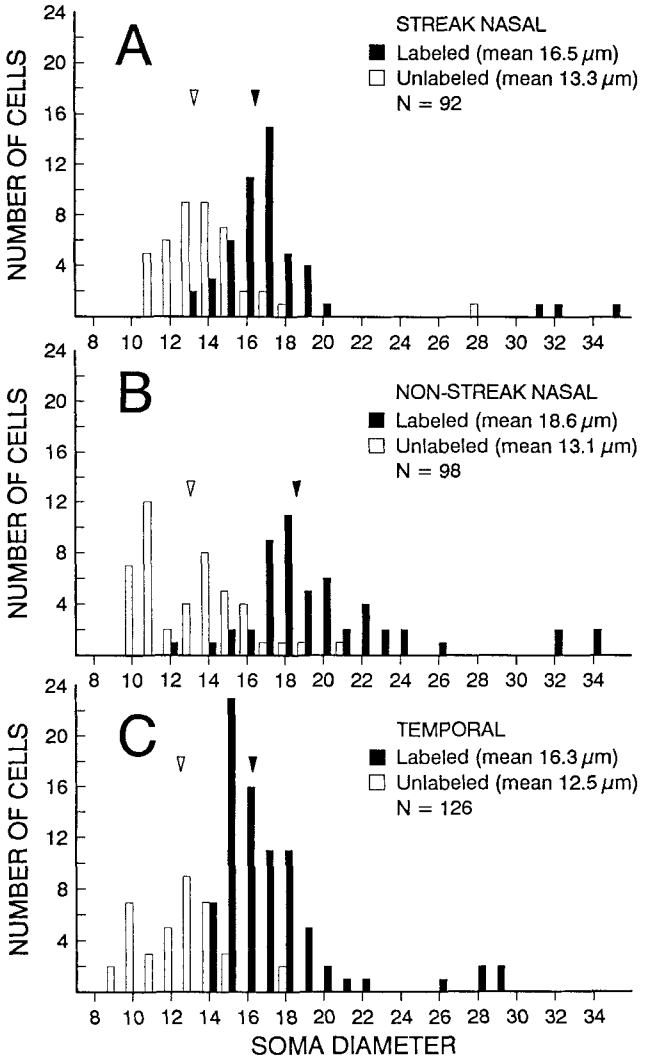

Fig. 11. Comparisons of soma size between labeled ganglion cells (filled bars) and unlabeled ones (open bars) at three retinal locations after bead deposits restricted to the A-layers of the LGN. Excluding the largest ganglion cells (> 24 μm diameter), labeled cells are presumably beta cells and unlabeled ones gamma cells. Most ganglion cells of intermediate size are labeled, as expected if all beta cells were labeled by these deposits. **A:** Nasal visual streak (cat G13L; same site as Fig. 10C). **B:** Nasal nonstreak retina (cat G13L; same site as Fig. 10D). **C:** Temporal retina (cat G13R; same site as Fig. 10B). Arrowheads indicate mean soma sizes for labeled and unlabeled cells (excluding alpha cells). Presumed beta cells (labeled nonalpha cells) are smaller on average in the visual streak (A) than in the nonstreak part of the same retina (B). Relatively small size of temporal beta cells (C) reflects pericentral retinal location of sample zone. Presumed gamma cells (unlabeled nonalpha cells) exhibit little topographic variation in size.

the coverage constant, which we will argue below may be an underestimate. Had a larger value been used, the map would have the same form but the density estimates would have been proportionally higher.

DISCUSSION

The present findings indicate that beta cells have a distinctive retinal distribution which includes a prominent nasal visual streak and disproportionately high densities in the central and temporal retina. They also show that dendritic field areas of beta cells are inversely proportional to local beta cell density so that about 4 beta cell fields overlap every retinal point.

The beta cell distribution: Validity of the present findings

Our perspective on the beta cell distribution represents a hybrid of several earlier formulations (see Introduction). On the one hand, our data support the view that this distribution differs from those of other ganglion cell classes (Peichl and Wässle, 1979; Rowe and Stone, 1976; Stone and Keens, 1980; Hughes, 1981b) including elevated beta cell fractions in the central (Peichl and Wässle, 1979; Hughes, 1981b) and temporal retina (Stone et al., 1980). On the other hand, our data do not confirm the view that beta cells are underrepresented in the visual streak (Rowe and Stone, 1976; Stone and Keens, 1980).

Discrepancies between our findings and earlier ones may stem from our identification of beta cells primarily by selective retrograde labeling rather than by soma size or partial dendritic filling. Our approach was predicated on the assumptions that the LGN A-layers receive input from all beta cells, and that beta and alpha cells are the only ganglion cell types projecting there. These assumptions are well-substantiated by observations on the receptive field properties of A-layer neurons and on the numbers, soma size, axon caliber and physiological response properties of afferent ganglion cells (for reviews see Lennie, 1980; Sherman and Spear, 1982; Stone, 1983; Sherman, 1985; Wässle and Boycott, 1991). Intracellular staining data of the present study confirmed that all ganglion cells with identified projections to the A-layers exhibit beta or alpha cell morphology.

Another assumption is that, at least locally, all and only the ganglion cells projecting to the A-layers exhibited retrograde labeling. It seems very likely that we locally labeled all the ganglion cells projecting to the A-layers, at least in experiments yielding the highest estimates of beta cell density (e.g., cats G1, G3, G9R, G9L, G10, G13L, G13R). Alpha cells, easily identified by their large somata, were almost invariably labeled in these experiments. Also, nearly all medium-sized ganglion cells were stained (Figs. 10 and 11), as would be expected if all beta cells were labeled. The exceptional unlabeled medium-sized cells were presumably gamma cells with soma sizes in the beta-cell range (Stone and Clarke, 1980; Leventhal et al., 1980; Pu et al., 1994; Stein and Berson, 1995).

Were the retrograde tracer deposits confined to the A-layers? In most bead experiments they clearly were. In others, one or two penetrations strayed beyond the A-layers, but the small retinal regions affected were excluded from our analysis. In the HRP studies, deposits were less clearly defined and may have involved the MIN, C-layers or LGNv to some degree. This should have labeled some gamma cells (Itoh et al., 1981; Rowe and Dreher, 1982; Leventhal et al., 1985; Pu and Berson, 1991) which would have been included in our counts and inflated estimated beta cell density. Surprisingly, density estimates were not consistently higher in the HRP experiments than in the bead studies. This implies either that geniculopetal gamma cells are relatively scarce (Leventhal et al., 1985; Pu and Berson, 1991; Pu et al., 1994) or that we labeled only a small fraction of them.

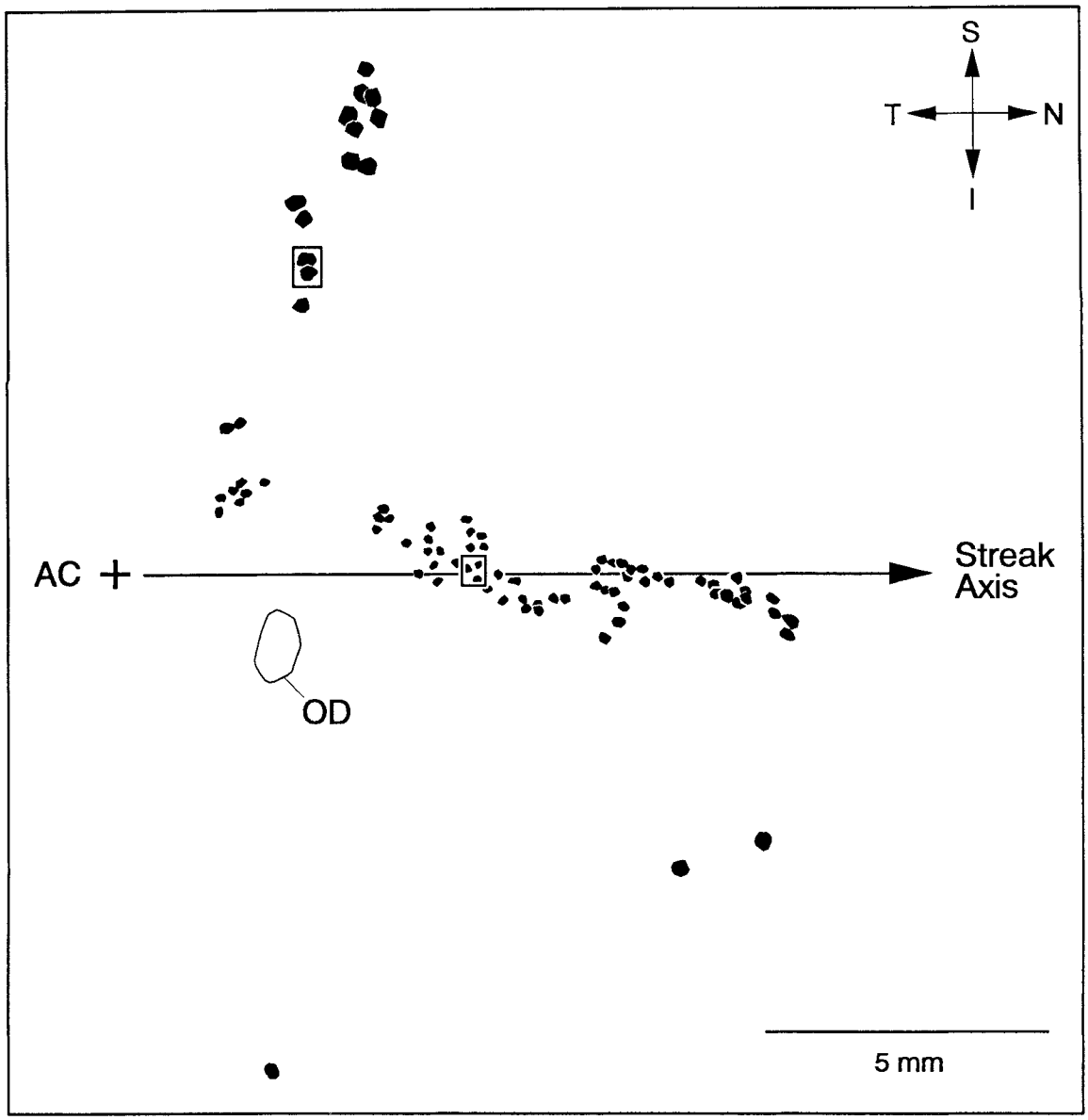

Fig. 12. Topographic variations in beta cell dendritic field dimensions in a single nasal hemiretina. Outlines represent the dendritic perimeters of beta cells stained by intracellular injection. These cells were also labeled by retrograde transport of fluorescent beads from the geniculate A-layers (experiment G8R). Dendritic fields increase in size with distance from the area centralis (AC, marked by +) and with distance from the visual streak, the axis of which is marked by the horizontal line (Streak Axis). Boxes indicate locations of cells in Figure 13. Beta cells on the streak also had smaller somas than those off the streak (see text). S, superior; I, inferior; T, temporal; N, nasal; OD, optic disk.

Several observations suggest that our maximal estimates approximate true beta cell density. For example, adding them to comparable independent estimates of alpha- and gamma cell density yields, as expected, values close to those for all ganglion cells (Figs. 7B, 8B). Presumed beta cells appear to account for at least half of all ganglion cells at most retinal locations (Figs. 7B, 8B), matching or exceeding earlier estimates of the beta cell fraction (Illing and Wässle, 1981; Hughes, 1981b; Leventhal, 1982; Stone, 1983). Finally, calculations based on our density estimates show that beta cell dendritic coverage is essentially constant over the retina (Fig. 15). Such uniformity seems highly unlikely to have arisen fortuitously from flawed estimates of density.

In some retinas, estimates of beta cell density were as much as 30% lower than the maximal estimates at matching locations in other retinas. Such variability is probably due mainly to failure to label some beta cells through incomplete saturation of the A-layers with tracer. However, we cannot exclude substantial interindividual differences in beta cell density or fraction. Despite the variation among cats, the general form of the distribution was consistent from animal to animal and in good agreement with that inferred from topographic variations in dendritic field area (Fig. 16). Thus, while the beta cell fraction may vary among cats in absolute terms, its topographic dependence appears quite consistent from cat to cat.

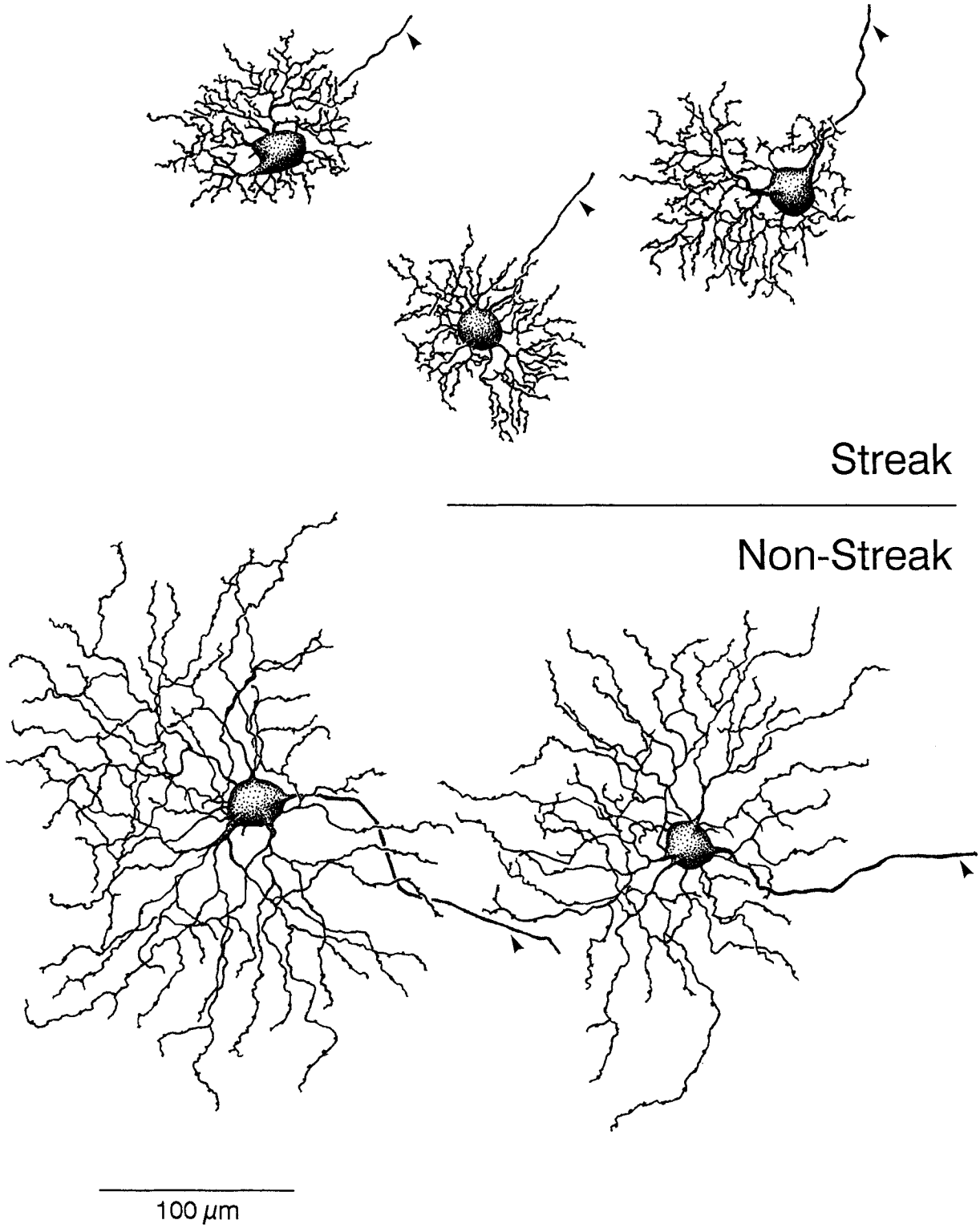

Fig. 13. Influence on beta cell morphology of cell's position relative to the visual streak. Camera lucida drawings show five of the intracellularly stained beta cells included in Figure 12. All five cells lay at an eccentricity of 30 degrees within a single retina. The three small-field cells at top lay within the visual streak, while the two large-field cells below lay in the superior retina more than 20 degrees away from the streak. See Figure 12 for topographic locations. Arrowheads indicate axons.

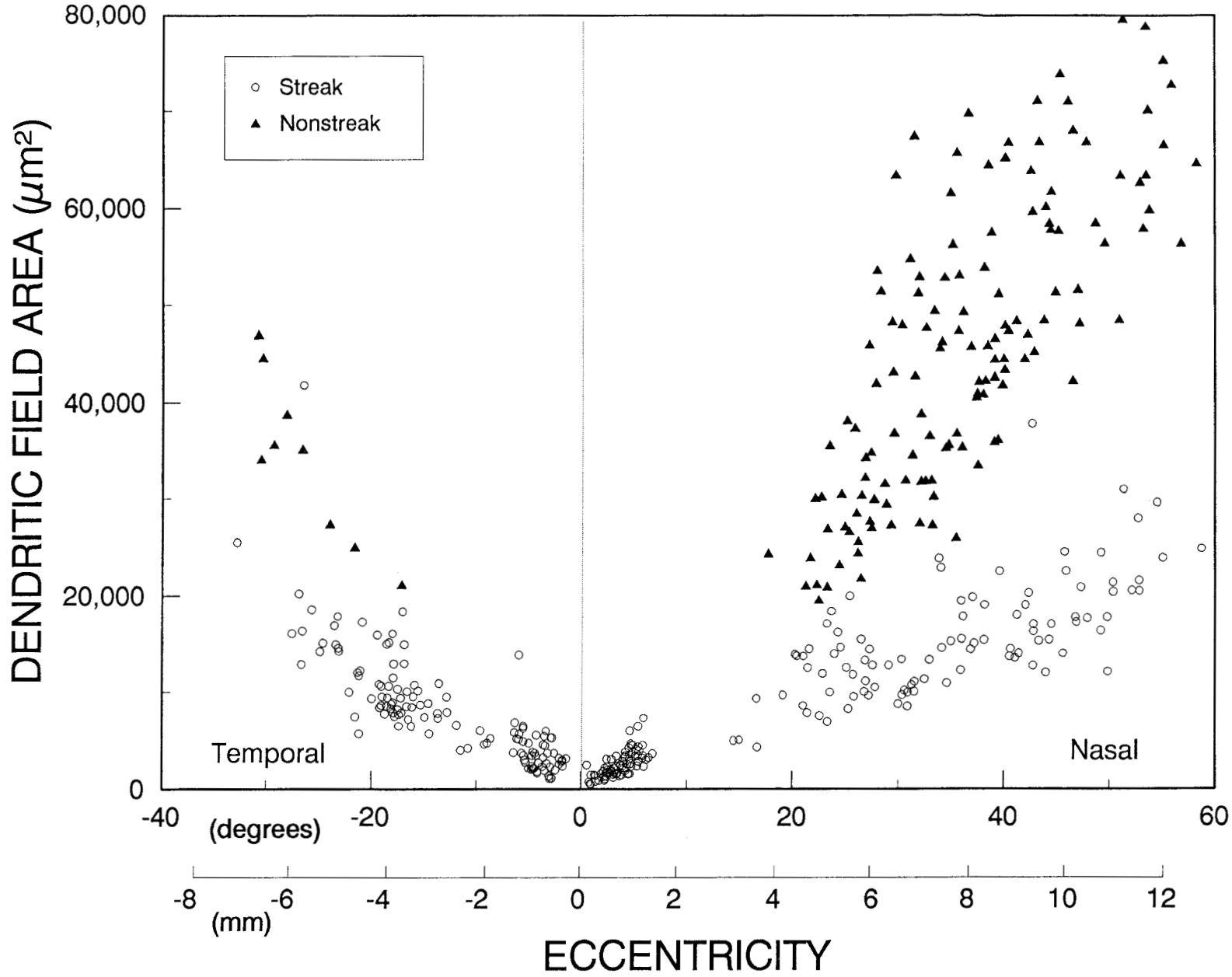

Fig. 14. Quantitative analysis of the effects of eccentricity, position relative to the visual streak, and nasotemporal location on beta cell dendritic field size. Beta cells lying within the visual streak (< 5 degrees from axis of nasal streak) are shown by the open circles; those lying well outside the streak (> 15 degrees from the streak axis) are shown by the filled triangles. By definition, there are no nonstreak cells at eccentricities < 15 degrees. For the temporal hemiretina, the streak axis was determined by extrapolation from the nasal retina. Beta cell dendritic fields are much smaller centrally than peripherally and smaller within the visual streak than at matching eccentricities outside it. Beta cells lying at intermediate positions relative to the streak (5–15 degrees from the streak axis; not shown) had intermediate dendritic field areas. Nasal and temporal hemiretinas differ only modestly in dendritic field size.

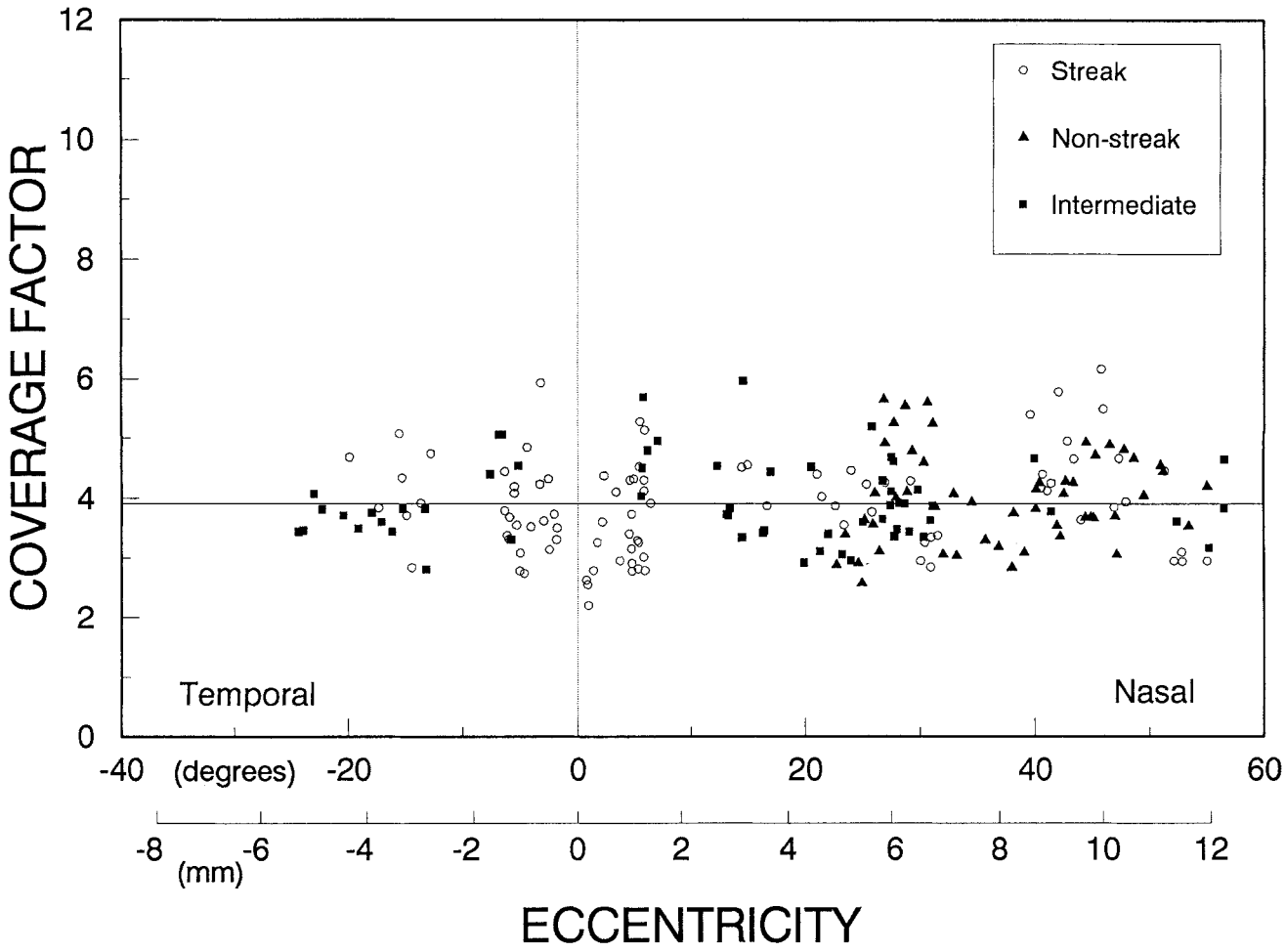

Fig. 15. Plot of anatomical coverage factor as a function of eccentricity for 204 intracellularly stained beta cells. Coverage was estimated for each cell as the product of its dendritic field area and the local beta cell density, determined by analysis of retrograde labeling patterns (see text). Coverage was independent of eccentricity, nasotemporal location, or position relative to the streak and averaged 3.93 (horizontal line). Cells were assigned to the streak (open circles), nonstreak retina (filled triangles) or intermediate position (filled squares) according to criteria described in text.

Incidence of beta cells in the central retina

Labeled presumed beta cells reached densities of 5,600–6,300 cells/mm^2 in the area centralis, but this may underestimate peak beta cell density. Ipsilaterally and contralaterally projecting beta cells are intermingled in the region of peak density (Stone, 1983), and our unilateral tracer deposits would have labeled only one of the two populations. The density of all ganglion cells peaks at about 10,000 cells/mm^2 in our material (see, e.g., Fig. 7 and Stein and Berson, 1995), a value as high as any reported in previous studies (Hughes, 1985). Taken together, the evidence suggests that beta cells account for at least 60% and perhaps as many as two-thirds of all ganglion cells in the area centralis. This inference is supported by direct evidence that at least 60% of all ganglion cells in the pericentral retina are nonalpha cells projecting to the A-layers (Figs. 9 and 10). Conversely, all nonbeta cells combined account for less than 40% of all ganglion cells in the central retina: about 35% of all cells are colliculopetal gamma cells (Stein and Berson, 1995) and $<5\%$ are alpha (Wässle et al., 1975).

Incidence of beta cells in the nasal periphery and visual streak

Our data indicate that beta cells represent a smaller fraction of ganglion cells in the nasal periphery (about 45–50%) than in the central retina (at least 60%). This is corroborated by a complementary gradient in the incidence of nonbeta cells, mainly gamma cells, which account for 45–50% of the ganglion cells in the nasal periphery as compared to only about 35% in the central retina (Stein and Berson, 1995; see also Hughes, 1981b). These topographic gradients in fractional representation may underlie the observation that X-cells are recorded relatively less frequently in the peripheral than in the central nasal retina, while the reverse is true for W-cells (Rowe and Stone, 1976; Hoffmann and Stone, 1985). Our findings conflict with those of Illing and Wässle (1981) who concluded that the beta cell fraction is essentially constant across the retina. The discrepancy may be traceable to methodological factors. For example, Illing and Wässle (1981) used thalamic tracer deposits that apparently extended well beyond the

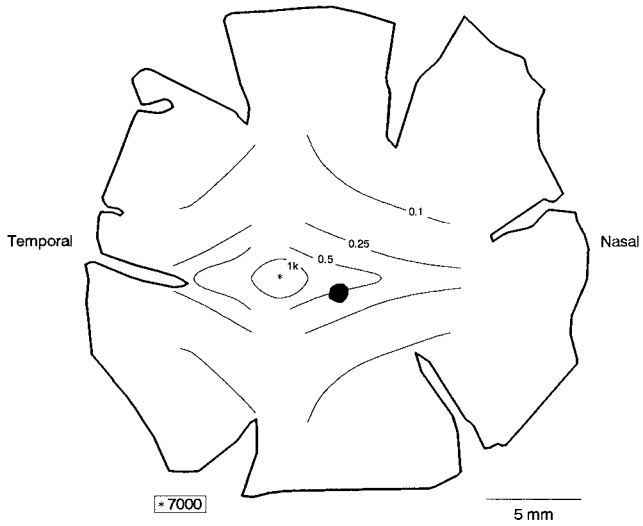

Fig. 16. Retinal distribution of beta cells as inferred from topographic variations in beta cell dendritic field size by assuming uniform anatomical coverage. Local beta cell density was estimated for each of 587 beta cells from 27 retinas by dividing a constant estimate of coverage (3.93) by the cell's dendritic field area. Isodensity map shown was drawn by eye from retinotopic plots of these density estimates. Data from superior and inferior retina were averaged so isodensity contours are symmetrical about the horizontal meridian. Estimates from dehydrated and cleared retinas did not differ appreciably from those from other retinas so no correction for differential shrinkage has been made. Schematic outlines of retina and optic disk are provided for orientation. Conventions as in Figure 2.

A-layers and relied on partial dendritic filling rather than selective retrograde transport to distinguish beta from gamma cells.

The nasal visual streak appears as prominent for the beta cell population as for cat ganglion cells generally so that the fraction of all ganglion cells that are beta cells is about the same inside the visual streak as elsewhere in the nasal periphery (Figs. 8B and 9). Hughes (1981b) reached the same conclusion based on evidence that the fraction of ganglion cells with soma sizes in the "beta mode" is the same in the nasal streak as in the nasal quadrants. Also consistent with this view is the finding that neonatal decortication, which results in preferential and widespread loss of beta cells, does not enhance the prominence of the visual streak relative to normal retinas (Rowe, 1990). As discussed in detail elsewhere (Stein and Berson, 1995), the disproportionately high frequency within the streak of small ganglion cells and of W-cell recordings (Rowe and Stone, 1976) appears largely attributable to a reduction in beta cell soma size in the streak (Hughes, 1981b; present findings) rather than to an increase in the gamma cell fraction there.

The tendency of beta cells to concentrate in the streak is reflected in their smaller dendritic fields there as compared to the nasal quadrants (Figs. 12–14; see also Peichl, 1992 for related anecdotal evidence in two other carnivores, the dog and wolf). This, in turn, presumably underlies the observation that X-cell receptive fields are 30% smaller in diameter within the visual streak than outside it (Rowe and Stone, 1976; Peichl and Wässle, 1979), since the dimensions of beta cell receptive fields and dendritic fields are correlated (Peichl and Wässle, 1979; but see Stanford, 1987). The concentration of beta cells within the streak may also be related to the pronounced anisotropy in linear magnification factors in the geniculate representation of the visual horizon (Sanderson, 1971).

Incidence of beta cells in the temporal retina

We have presented several lines of evidence that beta cells may constitute a larger fraction of all ganglion cells in the temporal retina (about two-thirds) than in the nasal periphery (about half). First, we compared estimated beta cell and total ganglion cell densities, in some cases within the same retina (Figs. 7, 9, and 10). Second, we showed that gamma cells exhibit the expected complementary nasotemporal difference in fractional representation (Stein and Berson, 1995). Third, we found that alpha cells, which form a fixed fraction of all ganglion cells, are outnumbered by presumptive beta cells more strongly in the temporal than in the nasal retina. Finally, we showed that, outside the central retina, the distribution of beta cells as inferred from retrograde transport (Figs. 2, 4 and 5) or dendritic field dimensions (Fig. 16) is more symmetric about the nasotemporal raphe than is the nasally biased distribution of all ganglion cells.

Several findings reported by Stone et al. (1980) are in accord with the proposed elevation in beta cell fraction temporally: medium-sized ganglion cells were relatively more common temporally than nasally (see also Stone and Keens, 1980); the X-cell-mediated field potential recorded at the optic disk was more prominent after shocks to the ipsilateral optic tract than after shocks to the contralateral tract; X-cell recordings were relatively more common among axons arising from the temporal retina than among axons of nasal origin; and beta cells were relatively more frequently encountered temporally than nasally among a sample of Golgi-stained neurons. On the other hand, Stone et al. (1980) did not observe significantly higher relative encounter rates for X-cell somatic recordings temporally than nasally. This might reflect interactions between electrode sampling bias and nasotemporal differences in the soma size of various ganglion cell classes. Also in apparent conflict with our claim is the observation of Hughes (1981b) that in the temporal retina, cells within the "beta mode" of the soma size spectrum make up no more than half of the "classic neurones" of the ganglion cell layer temporally. However, this finding is difficult to interpret given that the "classic neurones" of that study included a substantial population of displaced amacrine cells with relatively large somas (bar cells of Hughes, 1981b; Wong and Hughes, 1987).

Coverage

Our findings on the dimensions of beta cell dendritic fields are in general accord with those of earlier Golgi or intracellular staining studies (Boycott and Wässle, 1974; Kolb et al., 1981; Stanford, 1987; Dann et al., 1988), but indicate that dendritic field size is better predicted by local beta cell density than by eccentricity. According to our findings, beta cell coverage factor (local density × dendritic field area) is constant over the retina at about 4. Since there are nearly equal numbers of ON- and OFF-beta cells (Wässle et al., 1981a), this ensures that every point on the retina lies within the dendritic field of at least one, and typically two, beta cells of each center type.

The coverage estimates we obtained from individual beta cells exhibited considerable variability, ranging from roughly 2 to 6 (Fig. 15). A small part of this variability may be attributable to our lumping of ON-beta and OFF-beta

subtypes. These are known to form independent mosaics, with ON-betas exhibiting slightly lower densities and larger dendritic fields than the OFF-betas (Wässle et al., 1981a). A potentially larger source of variability is possible underestimation of beta cell densities in some locations through incomplete retrograde labeling or overestimation from inclusion of inadvertently labeled gamma cells. Because incomplete labeling seems the more likely error in the relevant bead experiments, we view the mean value of 4 to be a conservative estimate of aggregate beta cell coverage. A value of 6 may be taken as an upper bound for coverage, since individual beta cells never exhibited higher values even in experiments yielding maximal estimates of beta cell density. Although the scatter in coverage values seems partly attributable to such methodological factors, some of it may be real. In single retinas, neighboring beta cells varied in dendritic field area by as much as a factor of 2, a discrepancy far too large to attribute to differences between ON- and OFF-beta varieties or to the relatively shallow gradients in mean beta cell density. Of course, at such a small spatial scale, the fine structure of the beta cell mosaic becomes a critical factor. If the ON- and OFF-beta dendritic arrays manifest specific territorial interactions like those exhibited by other ganglion cell classes (Wässle et al., 1981b; Dacey, 1989, 1993; Vaney, 1994), the variability in field size could simply reflect local irregularities in the mosaic. Thus, the number of beta cell dendritic fields overlapping every retinal point might be more tightly regulated than evident from our analysis.

Of the three previous investigations of coverage by beta or X cells in the cat retina, none has reported retinotopic invariance. Peichl and Wässle (1979) estimated that physiological coverage (receptive field center area × density) remained fairly constant outside the central retina at 7–10, but rose sharply to 30 in the area centralis. Diameters of X-cell receptive field centers appear to be larger than those of beta cell dendritic fields by a factor of 1.5 (Wässle and Boycott, 1991) to 1.8 (based on a comparison of "critical band" data in Peichl and Wässle's Fig. 7 with our Fig. 14). Peichl and Wässle's physiological data thus imply anatomical coverages of 2.2–4.4 peripherally and 9–13 centrally. Wässle et al. (1981a) estimated a total beta cell anatomical coverage of 5.9 at a single peripheral temporal site (2.8 for ON-betas; 3.1 for OFF-betas) from Golgi data on dendritic fields and density estimates derived from retrograde labeling and partial dendritic filling. Leventhal (1982) used a similar approach, except that dendritic field measurements were made from retrograde HRP staining of the dendrites, and estimated beta coverage at about 3–6 peripherally and about 10 centrally. Thus, our estimates are largely in keeping with earlier estimates of beta cell coverage peripherally, but are substantially lower centrally. The steep density gradients in central retina make coverage estimates there especially vulnerable to errors when trying to relate dendritic or receptive field data from one retina with density values from another. We were able to avoid such difficulties by making estimates of both local density and field size for individual beta cells within a single retina.

Approximate uniformity of coverage has previously been reported for two other classes of cat ganglion cells: alpha cells (Peichl and Wässle, 1979; Wässle et al., 1981b) and the monoamine-accumulating type (Dacey, 1989). The values of coverage are rather similar for the three classes when one considers single center subtypes. Coverage for is 1.4 for ON-alphas, 1.7 for OFF-alphas (Wässle et al., 1981b), and 2.2 for the monoamine-accumulating cells (apparently exclusively OFF-type; Dacey, 1989). ON- and OFF-beta cells each have a coverage of about 2 (present data), assuming roughly equal numbers of ON- and OFF-beta cells (Wässle et al., 1981a).

Sampling theory and spatial resolution

The topographic constancy of coverage among beta cells may reflect an optimization of the beta cell array for spatial resolution. According to sampling theory, the spacing of cells in a retinal mosaic determines its Nyquist limit, the highest spatial frequency that the array can accurately signal to the brain (e.g., Snyder and Miller, 1977; Hughes, 1981a; Wässle and Boycott, 1991). However, the bandpass of the array is also determined by the spatial frequency response of its constituent elements, that is, by the resolution of the individual ganglion cells. In an ideal system, the cutoff frequency of the ganglion cells would be matched to the Nyquist frequency, for if it were lower (oversampling), information theoretically available in the sampling array would be lost, and if it were higher (undersampling), the system would be vulnerable to aliasing.

Although the relevance of such abstractions to biological visual systems viewing natural scenes is debatable (e.g., see below), the beta cell system seems a reasonable fit to the ideal system just outlined. The Nyquist wavelength of a regular array is proportional to the intercell distance, so the same should be true for resolution (the smallest resolvable spatial period) in an optimized ganglion cell system. If dendritic field diameters are, in turn, proportional to resolution (Peichl and Wässle, 1979; Wässle and Boycott, 1991; but see Stanford, 1987), they should also be proportional to intercell spacing. Thus, anatomical (as well as physiological) coverage should be constant. According to our data, beta cells not only meet these minimal conditions for matching resolution to the Nyquist limit, but further exhibit a value for coverage close to that predicted for such an ideal system. To obtain the predicted value of coverage, let us assume that beta cell resolution matches the Nyquist limit of a hexagonal array, namely, 1.73 times the intercell spacing (Wässle and Boycott, 1991). X-cell (beta cell) resolution is 0.56 times the receptive field center diameter (Wässle and Boycott, 1991) which, in turn, is 1.5–1.8 times the dendritic field diameter (see above). This predicts that beta cell dendritic field diameters should be 1.72–2.06 times the intercell spacing in an ideal system. Intercell spacing for a hexagonal array is $\sqrt{(2/(d\sqrt{3}))}$ where d is cell density (Peichl and Wässle, 1976), so anatomical coverage is $(\pi k^2)/(2\sqrt{3})$ where k is the dendritic field diameter expressed as a multiple of intracellular distance. Thus, the foregoing estimated range for k (1.72–2.06) predicts an anatomical coverage of 2.67–3.84 for an ideal beta cell system, values close to that we obtained empirically. A similar correspondence was reported by Hughes (1981a) who pooled the ON- and OFF-beta subpopulations as we did, and by Wässle and Boycott (1991) who treated these subpopulations independently.

Implications for visual acuity

It is widely assumed that the limit for cat spatial acuity is set by the spatial resolution of X-cells (e.g., Lennie, 1980; Stone, 1983; Sherman and Spear, 1985; Sherman, 1985). If, as just suggested, X-cell resolution is in turn matched to the beta cell array, the cat's ability to resolve fine spatial detail may be a simple function of the mean local spacing of beta cells. This is obviously an oversimplified view. For example,

it ignores the obvious departure of the beta cell array from a regular hexagonal lattice, especially when the ON- and OFF-beta mosaics are combined (Wässle et al., 1981a), and the possible integrative contributions of the central visual pathways. Nonetheless, the upper bound for cat spatial acuity estimated by behavioral or evoked-potential methods (8.5–9.5 cycles/degree; Mitchell et al., 1977; Harris, 1978) closely matches the Nyquist limit of 9.4 cycles/degree calculated for the beta cell array at the area centralis (assuming a hexagonal array at a density of 6,500 cells/mm^2).

If cat spatial acuity is set by beta cell spacing, the present findings engender three predictions. First, in the nasal retina (temporal hemifield), acuity should rise more steeply with proximity to the center of gaze than would be predicted were acuity related instead to the densities of all ganglion cells. Second, acuity in the temporal retina should be more nearly matched to that in the nasal retina than would be predicted from the overall ganglion cell distribution, with its relatively large nasotemporal density imbalance. Finally, spatial resolution should fall off less steeply with eccentricity along the horizon (visual streak) than in the upper or lower nasal retinal quadrants. The behavioral data of Pasternak and Horn (1991) are consistent with the first two of these predictions, although silent on the third. Assuming that resolution is proportional to intercell spacing, acuity at a retinal eccentricity of 32 degrees nasal would be 37% of that at the center of gaze if it were limited by total ganglion cell density (10,000 vs. 1,400 cells/mm^2) but only 32% if it were limited by beta cell density (6,200 vs. 650 cells/mm^2; Fig. 7A). Behaviorally measured acuity was 28% of that centrally, close to that predicted from the beta cell distribution. At an eccentricity of 16 degrees, acuity of the temporal retina should be only 75% that at the same eccentricity nasally if it were limited by total ganglion cell density, but 83% if limited by the beta cell mosaic. The behavioral value was 85%.

Relationship to primate retina

It has been suggested that the beta (X) cell system of the cat retina is analogous to the midget cell (P-cell; P-beta) system of the primate retina (Leventhal et al., 1981; Rodieck et al., 1985; Dacey and Brace, 1992), although this remains controversial (Shapley and Perry, 1986). The present results, while hardly definitive, lend weight to the analogy. Human midget cells are disproportionately represented in the central retina, representing perhaps more than 90% of ganglion cells there, as compared to less than 50% in the periphery (Dacey and Petersen, 1992; Dacey, 1993) and a similar pattern has been suggested for nonhuman primates, although this has been disputed (Perry et al., 1984; Schein and deMonasterio, 1987). We find a parallel (though less marked) preponderance of beta cells in the central retina. Primate midget cells may also represent an increased fraction of ganglion cells in the temporal retina (Watanabe and Rodieck, 1989), just as we have observed for cat beta cells. Finally, midget cells in humans (Dacey, 1993) and probably also in macaques (Watanabe and Rodieck, 1989) exhibit constant anatomical coverage just as cat beta cells do. However, the suggestion that cat beta cells might have a "primate-like" radially symmetric distribution (Rowe and Stone, 1976; Stone and Keens, 1980; Rowe, 1990) is at odds with the present evidence for a prominent visual streak. This can be added to the ample list of features distinguishing cat beta (X) cells from primate midget (P) cells, including their lack of color opponency, their poorer spatial resolution, and their lower absolute numbers. It remains unclear whether such distinctions reflect evolutionary divergence of homologous cell classes or simply a lack of homology.

ACKNOWLEDGMENTS

We thank Mingliang Pu for providing some of the intracellularly stained beta cells and advice on bulk filling of ganglion cells. We thank James McIlwain, Mike Paradiso, and Peter Biancani for donations of normal cat retinas. This work was supported by NIH R01 EY06108.

LITERATURE CITED

Berson, D.M., and J.J. Stein (1995) Retinotopic organization of the superior colliculus in relation to the retinal distribution of afferent ganglion cells. Visual Neurosci. *12*:671–686.

Boycott, B.B., and H. Wässle (1974) The morphological types of ganglion cells of the domestic cat's retina. J. Physiol. (Lond) *240*:397–419.

Cleland, B.G., W.R. Levick, and K.J. Sanderson (1973) Properties of sustained and transient ganglion cells in the cat retina. J. Physiol. (Lond.) *228*:649–680.

Cleland, B.G., W.R. Levick, R. Morstyn, and H.G. Wagner (1976) Lateral geniculate relay of slowly conducting retinal afferents to cat visual cortex. J. Physiol. (Lond.) *255*:299–320.

Dacey, D.M. (1989) Monoamine-accumulating ganglion cell type of the cat's retina. J. Comp. Neurol. *288*:59–80.

Dacey, D.M. (1993) The mosaic of midget ganglion cells in the human retina. J. Neurosci. *13*:5334–5355.

Dacey, D.M., and S. Brace (1992) A coupled network for parasol but not midget ganglion cells in the primate retina. Visual Neurosci. *9*:279–290.

Dacey, D.M., and M.R. Petersen (1992) Dendritic field size and morphology of midget and parasol ganglion cells of the human retina. Proc. Natl. Acad. Sci. USA *89*:9666–9670.

Dann, J.F., E.H. Buhl, and L. Peichl (1988) Postnatal dendritic maturation of alpha and beta cells in cat retina. J. Neurosci. *8*:1485–1499.

Fischer, B. (1973) Overlap of receptive field centers and representation of the visual field in the cat's optic tract. Vision Res. *13*:2113–2120.

Fukuda, Y., and J. Stone (1974) Retinal distribution and central projections of Y-, X-, and W-cells of the cat's retina. J. Neurophysiol. *37*:749–772.

Guillery, R.W., E.E. Geisert, Jr., E.H. Polley, and C.A. Mason (1980) An analysis of the retinal afferents to the cat's medial interlaminar nucleus and to its rostral thalamic extension, the "geniculate wing." J. Comp. Neurol. *194*:117–142.

Hanker, J.S., P.E. Yates, C.B. Meltz, and A. Rustioni (1977) A new specific sensitive and noncarcinogenic reagent for the demonstration of horseradish peroxidase. J. Histochem. Cytochem. *9*:789–792.

Harris, L.R. (1978) Contrast sensitivity and acuity of a conscious cat measured by the occipital evoked potential. Vision Res. *18*:175–178.

Hoffmann, K.-P., and J. Stone (1985) Retinal input to the nucleus of the optic tract of the cat assessed by antidromic activation of ganglion cells. Exp. Brain Res. *59*:395–403.

Hsiao, C.-F., and S.M. Sherman (1986) Alpha and beta cells projecting from retina to lamina A of the lateral geniculate nucleus in normal cats, monocularly deprived cats, and young kittens. Exp. Brain Res. *61*:413–431.

Hughes, A. (1981a) Cat retina and the sampling theorem; The relation of transient and sustained brisk-unit cut-off frequency to alpha and beta-mode cell density. Exp. Brain Res. *42*:196–202.

Hughes, A. (1981b) Population magnitudes and distribution of the major modal classes of cat retinal ganglion cells as estimated from HRP filling and a systematic survey of the soma diameter spectra for classical neurones. J. Comp. Neurol. *197*:303–340.

Hughes, A. (1985) New perspectives in retinal organisation. In N.N. Osborne and G.J. Chader (eds): Progress in Retinal Research. Vol. 4. Oxford: Pergamon Press, pp. 243–313.

Illing, R.-B., and H. Wässle (1981) The retinal projection to the thalamus in the cat: A quantitative investigation and a comparison with the retinotectal pathway. J. Comp. Neurol. *202*:265–285.

Itoh, K., M. Conley, and I.T. Diamond (1981) Different distributions of large and small ganglion cells in the cat after HRP injections of single layers of the lateral geniculate body and the superior colliculus. Brain Res. *207:*147–152.

Kelly, J.P., and C.D. Gilbert (1975) The projections of different morphological types of ganglion cells in the cat retina. J. Comp. Neurol. *163:*65–80.

Kolb, H., R. Nelson, and A. Mariani (1981) Amacrine cells, bipolar cells and ganglion cells of the cat retina: A Golgi study. Vision Res. *21:*1081–1114.

Lachica, E.A., J.A. Mavity-Hudson, and V.A. Casagrande (1991) Morphological details of primate axons and dendrites revealed by extracellular injection of biocytin: An economic and reliable alternative to PHA-L. Brain Res. *564:*1–11.

Lennie, P. (1980) Parallel visual pathways. Vision Res. *20:*561–594.

Leventhal, A.G. (1982) Morphology and distribution of retinal ganglion cells projecting to different layers of the dorsal lateral geniculate nucleus in normal and Siamese cats. J. Neurosci. *2:*1024–1042.

Leventhal, A.G., J. Keens, and I. Törk (1980) The afferent ganglion cells and cortical projections of the retinal recipient zone (RRZ) of the cat's 'pulvinar complex'. J. Comp. Neurol. *194:*535–554.

Leventhal, A.G., R.W. Rodieck, and B. Dreher (1981) Retinal ganglion cell classes in the Old World monkey: morphology and central projections. Science *213:*1139–1142.

Leventhal, A.G., R.W. Rodieck, and B. Dreher (1985) Central projections of cat retinal ganglion cells. J. Comp. Neurol. *237:*216–226.

Mitchell, D.E., F. Griffin, and B. Tinney (1977) A behavioural technique for the rapid assessment of visual capabilities of kittens. Perception *6:*181–193.

Pasternak, T., and K. Horn (1991) Spatial vision of the cat: Variation with eccentricity. Visual Neurosci. *6:*151–158.

Peichl, L. (1992) Morphological types of ganglion cells in the dog and wolf retina. J. Comp. Neurol. *324:*590–602.

Peichl, L., and H. Wässle (1979) Size, scatter, and coverage of ganglion cell receptive field centers in the cat retina. J. Physiol. (Lond.) *291:*117–141.

Perry, V.H., R. Oehler, and A. Cowey (1984) Retinal ganglion cells that project to the dorsal lateral geniculate nucleus in the macaque monkey. Neuroscience *12:*1101–1123.

Pu, M., and D.M. Berson (1991) Morphology of ganglion cells innervating the medial interlaminar nucleus of the lateral geniculate body. Soc. Neurosci. Abstr. *17:*709.

Pu, M., and D.M. Berson (1992) A method for reliable and permanent intracellular staining of retinal ganglion cells. J. Neurosci. Methods *41:*45–51.

Pu, M., D.M. Berson, and T. Pan (1994) Structure and function of retinal ganglion cells innervating the cat's geniculate wing: An in vitro study. J. Neurosci. *14:*4338–4358.

Rodieck, R.W., K.F. Binmoeller, and J. Dineen (1985) Parasol and midget ganglion cells of the human retina. J. Comp. Neurol. *233:*115–132.

Rowe, M.H. (1990) Evidence for degeneration of retinal W cells following early visual cortical removal in cats. Brain Behav. Evol. *35:*253–267.

Rowe, M.H., and B. Dreher (1982) Retinal W-cell projections to the medial interlaminar nucleus in the cat: Implications for ganglion cell classification. J. Comp. Neurol. *204:*117–133.

Rowe, M.H., and J. Stone (1976) Properties of ganglion cells in the visual streak of the cat's retina. J. Comp. Neurol. *169:*99–126.

Sanderson, K.J. (1971) The projection of the visual field to the lateral geniculate and medial interlaminar nuclei in the cat. J. Comp. Neurol. *143:*101–118.

Schein, S.J., and F.M. de Monasterio (1987) Mapping of retinal and geniculate neurons onto striate cortex of macaque. J. Neurosci. *7:*996–1009.

Schmued, L.C., L.W. Swanson, and P.E. Sawchenko (1982) Some fluorescent counterstains for neuroanatomical studies. J. Histochem. Cytochem. *30:*123–128.

Shapley, T., and V.H. Perry (1986) Cat and monkey retinal ganglion cells and their visual functional roles. Trends Neurosci. *9:*229–235.

Sherman, S.M. (1985) Functional organization of the W-, X-, and Y-cell pathways in the cat: A review and hypothesis. Prog. Psychobiol. Physiol. Psychol. *11:*233–314.

Sherman, S.M., and P.D. Spear (1982) Organization of visual pathways in normal and visually deprived cats. Physiol. Rev. *62:*738–855.

Snyder, A.W., and W.H. Miller (1977) Photoreceptor diameter and spacing for highest resolving power. J. Opt. Soc. Am. *67:*696–698.

Stanford, L.R. (1987) X-cells in the cat retina: Relationships between the morphology and physiology of a class of cat retinal ganglion cells. J. Neurophysiol. *58:*940–964.

Stein, J.J., and D.M. Berson (1995) On the distribution of gamma cells in the cat retina. Visual Neurosci. *12:*687–700.

Stone, J. (1978) The number and distribution of ganglion cells in the cat's retina. J. Comp. Neurol. *180:*753–772.

Stone, J. (1983) Parallel Processing in the Visual System: The Classification of Retinal Ganglion Cells and its Impact on the Neurobiology of Vision. New York: Plenum Press.

Stone, J., and R. Clarke (1980) Correlation between soma size and dendritic morphology in cat retinal ganglion cells: Evidence of further variation in the gamma-cell class. J. Comp. Neurol. *192:*211–217.

Stone, J., and J. Keens (1980) Distribution of small and medium-sized ganglion cells in the cat's retina. J. Comp. Neurol. *192:*235–246.

Stone, J., A. Leventhal, C.R.R. Watson, J. Keens, and R. Clarke (1980) Gradients between nasal and temporal areas of the cat retina in the properties of retinal ganglion cells. J. Comp. Neurol. *192:*219–233.

Vakkur, G.J., P.O. Bishop, and W. Kozak (1963) Visual optics in the cat, including posterior nodal distance and retinal landmarks. Vision Res. *3:*289–314.

Vaney, D.I. (1994) Territorial organization of direction-selective ganglion cells in rabbit retina. J. Neurosci. *14:*6301–6316.

Wässle, H., and B.B. Boycott (1991) Functional architecture of the mammalian retina. Physiol. Rev. *71:*447–480.

Wässle, H., W.R. Levick, and B.G. Cleland (1975) The distribution of the alpha type of ganglion cells in the cat's retina. J. Comp. Neurol. *159:*419–437.

Wässle, H., B.B. Boycott, and R.-B. Illing (1981a) Morphology and mosaic of on- and off-beta cells in the cat retina and some functional considerations. Proc. R. Soc. Lond. [Biol.] *212:*177–195.

Wässle, H., L. Peichl, and B.B. Boycott (1981b) Morphology and topography of on- and off-alpha cells in the cat retina. Proc. R. Soc. Lond. [Biol.] *212:*157–175.

Watanabe, M., and R.W. Rodieck (1989) Parasol and midget ganglion cells of the primate retina. J. Comp. Neurol. *289:*434–454.

Wong, R.O.L., and A. Hughes (1987) The morphology, number, and distribution of a large population of confirmed displaced amacrine cells in the adult cat retina. J. Comp. Neurol. *255:*159–177.